


Article

# Questions of Mirror Symmetry at the Photoexcited and Ground States of Non-Rigid Luminophores Raised by Circularly Polarized Luminescence and Circular Dichroism Spectroscopy: Part 1. Oligofluorenes, Oligophenylenes, Binaphthyls and Fused Aromatics

Michiya Fujiki <sup>1,\*</sup> , Julian R. Koe <sup>2,\*</sup>, Takashi Mori <sup>1</sup> and Yoshihiro Kimura <sup>1</sup>

<sup>1</sup> Division of Materials Science, Graduate School of Science and Technology, Nara Institute of Science and Technology (NAIST), 8916-5 Takayama, Ikoma, Nara 630-0036, Japan; mori@tri-osaka.jp (T.M.); yoshi19791024uk@gmail.com (Y.K.)

<sup>2</sup> Department of Natural Sciences, International Christian University (ICU), 3-10-2 Mitaka, Tokyo, 181-8585, Japan

\* Correspondence: fujikim@ms.naist.jp (M.F.); koe@icu.ac.jp (J.R.K.); Tel.: +81-743-72-6040 (M.F.); +81-422-33-3249 (J.R.K.)

Received: 12 September 2018; Accepted: 6 October 2018; Published: 11 October 2018



**Abstract:** We report experimental tests of whether non-rigid,  $\pi$ -conjugated luminophores in the photoexcited ( $S_1$ ) and ground ( $S_0$ ) states dissolved in achiral liquids are mirror symmetrical by means of circularly polarized luminescence (CPL) and circular dichroism (CD) spectroscopy. Herein, we chose ten oligofluorenes, eleven linear/cyclic oligo-*p*-arylenes, three binaphthyls and five fused aromatics, substituted with alkyl, alkoxy, phenyl and phenylethynyl groups and also with no substituents. Without exception, all these non-rigid luminophores showed negative-sign CPL signals in the UV-visible region, suggesting temporal generation of energetically non-equivalent non-mirror image structures as far-from equilibrium open-flow systems at the  $S_1$  state. For comparison, unsubstituted naphthalene, anthracene, tetracene and pyrene, which are achiral, rigid, planar luminophores, did not obviously show CPL/CD signals. However, camphor, which is a rigid chiral luminophore, showed mirror-image CPL/CD signals. The dissymmetry ratio of CPL ( $g_{lum}$ ) for the oligofluorenes increased discontinuously, ranging from  $\approx -(0.2 \text{ to } 2.0) \times 10^{-3}$ , when the viscosity of the liquids increased. When the fluorene ring number increased, the  $g_{lum}$  value extrapolated at  $[\eta] = 0$  reached  $-0.8 \times 10^{-3}$  at 420 nm, leading to (–)-CPL signals predicted in the vacuum state. Our comprehensive CPL and CD study should provide a possible answer to the molecular parity violation hypothesis arising due to the weak neutral current mediated by the  $Z^0$ -boson.

**Keywords:** circularly polarized luminescence; circular dichroism; symmetry breaking; parity violation; weak neutral current; tunneling;  $Z^0$  boson; fluorene; camphor; binaphthyl; laser dyes

## 1. Introduction

Quantum mechanics (QM) relies on the electromagnetic (EM) force mediated by the massless photon ( $\gamma$ ). QM affords the novel hypothesis that true mirror-image molecules are not observable at stationary states [1–3]. In 1927, Hund posed a fundamental question referred to as Hund's paradox, which concerns the relationship between optical activity and molecular chirality in a symmetrical potential energy double-well (DW). Because of quantum tunneling, mirror-image molecules are

described by superposition of the odd- and even-parity eigenstates,  $|L\rangle = 1/\sqrt{2} (|+\rangle - |-\rangle)$  and  $|R\rangle = 1/\sqrt{2} (|+\rangle + |-\rangle)$  or vice versa [1–3]. However, because of the parity-conservation law in energetically equivalent mirror-image molecules, the tunneling time between two local minima separated by a potential barrier ( $E_b$ ) is inversely proportional to the energy splitting  $\Delta E_{\pm}$  between the odd- and even-parity eigenstates. When the  $E_b$  value is sufficiently low, the molecules spontaneously oscillate between the  $|L\rangle$  and  $|R\rangle$  states, leading to the novel concept of *spatiotemporal chirality*. In tri-substituted phosphines,  $P\text{-}R_1R_2R_3$ ,  $E_b \approx 37 \text{ kcal mol}^{-1}$  and the tunneling splitting,  $\Delta E_{\pm}$ , is of the order of  $10^{-17} \text{ eV}$  [2], so the quantum oscillation of optical activity cannot be detected. On the other hand, because the inversion barrier of ammonia due to quantum tunneling is around  $5.8 \text{ kcal mol}^{-1}$ , a  $\Delta E_{\pm}$  of  $0.8 \text{ cm}^{-1}$  is observable [4]. Ammonia molecules thus spontaneously oscillate with time, in a temperature-independent flip-flop motion via a tunneling mechanism.

In 1956, Lee and Yang suggested from a theoretical standpoint that the parity conservation law in certain nuclear reactions, due to the weak nuclear force, was not yet proved [4]. Wu et al. and other workers verified the parity violation (PV) hypothesis at the sub-atomic level in a series of  $\beta^-$ - and  $\beta^+$ -decay experiments of several radioactive sources [5–10]. These results stimulated other work, resulting in what is known as the electroweak (EW) theory, to unify the PV weak and parity-conserving EM forces in the 1960s [11]. In 1983, massive charged  $W^{\pm}$  ( $\sim 80 \text{ GeV}$ ) bosons and the neutral  $Z^0$  boson ( $\sim 91 \text{ GeV}$ ) were indeed detected at CERN [12–15].

PV effects at sub-atomic level were successfully detected during spontaneous nuclear emission processes. The  $\beta^-$ -decay of  $^{60}\text{Co} \rightarrow ^{60}\text{Ni}$  mediated by the  $W^-$  boson radiates a left-handed electron (0.317 MeV), left-handed circularly polarized  $\gamma$ -rays (1.173 GeV and 1.332 GeV) and a right-handed anti-neutrino ( $< 2 \text{ eV}$ ) [16]; conversely, the  $\beta^+$ -decay in  $^{58}\text{Co} \rightarrow ^{58}\text{Fe}$  by the  $W^+$  boson releases a right-handed positron (0.475 MeV), a right-handed circularly polarized  $\gamma$ -ray (0.811 GeV) and a left-handed neutrino [12].

The EW force mediated by the  $Z^0$  boson further predicated the induction of hidden optical activity in all atoms because of left-handed  $Z^0$  [17,18]. Actually, optical activity of atomic vapors (Pb, Tl, Bi, Cs, Yb and others) [19–26] and solid metal ( $^{117}\text{Sn}$ ) [27] has been detected as an atomic parity violation (APV) [19–27]. The optical activity of the atomic vapors has a dissymmetry ratio ( $g$ )  $\approx -10^{-7}$  associated with an anapole moment in the visible and near-IR regions characterized by optical rotation dispersion (ORD) and electric field-induced absorption and polarized luminescence (CPL) spectra [18–26]. Compared to electric field-induced absorption experiments, the profound APV effects of Cs and Tl vapors in the photoexcited state at the forbidden transitions are more sensitively detectable as CPL and PL signals [20,22,23] and also that of Yb vapors was boosted by two orders of magnitude using AC-Stark induced second harmonic transitions under a static magnetic field [26].

Additionally, since the early 1970s and 1980s, several theoreticians have invoked the molecular parity violation (MPV) hypothesis from the viewpoint of hierarchical matter world in our Universe: the parity-violating weak neutral current (PV-WNC) in the electron–nuclei interactions mediated by the  $Z^0$ -boson stabilizes one of the mirror-image molecules and conversely destabilizes the other [1,2,28–39]. The MPV hypothesis predicts that conventional mirror-image molecules are thus no longer enantiomers and should behave as diastereomers due to parity violating energy shifts (PVES), in which  $+E_{PV}$  for one and  $-E_{PV}$  for another, now popularly called parity violating energy difference (PVED),  $\Delta E_{PV}$  or simply  $E_{PV}$  are evident. The hypothesis definitively contradicts modern stereochemistry as described in textbooks and lecture notes. However, most MPV theories [1,2,28–50] have estimated that the value of  $E_{PV}$  between mirror-image molecules are vanishingly small: of the order of  $10^{-8}$ – $10^{-14} \text{ kcal mol}^{-1}$ . These  $E_{PV}$  values are equivalent to an excess of one L- (or R-) molecule in a racemic mixture of  $10^{11}$ – $10^{17}$  molecules ( $10^{-9}$ – $10^{-15}\%$  ee), therefore, beyond the detection capabilities of ordinary UV-visible, IR and NMR spectrometers and chromatographic instruments available in typical laboratories. Even if the MPV hypothesis is valid, one cannot at all recognize the difference between enantiomers and agrees that the enantiomers obey the stereochemistry descriptions in the textbooks.

However, several amplification scenarios of *PVED* have been postulated, leading to spectroscopically detectable levels.

For example, Yamagata first proposed an accumulation model in which the faint  $E_{PV}$  is linearly amplified by the association of molecules into chain-like polymers and/or solid crystals [28]. Harris and Stodolsky assumed that the *PC-EM*-originating quantum oscillation of hypothetical chiral molecules in a DW is slightly influenced by *PV*-originating oscillation [34]. Other theoretical models of realistic molecules were discussed by Hegstrom et al. (twisted ethylene) [35], Macdermott and Hegstrom (ammonia-like molecules) [47], Mason and Tranter (glycine and polyglycine) [36] and Kikuchi et al. (*n*-alkanes) [43]. Salam predicted that the second-order phase-transition of a molecular system, as exemplified by amino acids, spontaneously shows a handed mirror symmetry breaking (MSB) at  $T_c \sim 250$  K [41]. Quack showed that high-resolution ro-vibrational spectroscopy is useful to detect the *PVED* of around 40 realistic and hypothetical molecules [2,48,49]. Schwerdtfeger et al. showed that subtle  $E_{PV}$  effects are enhanceable with the help of relativistic effects in heavier atoms [47,50]. P. Bargeño et al. simulated decoherence behaviors of dissipative chiral molecules in two-level systems, when tunneling and parity violation effects are opposed [51].

Quack et al. [46,49] and Macdermott and Hegstrom [48] discussed three representative cases of (i)  $E_{PV} \gg E_{\pm}$ , (ii)  $E_{PV} \ll E_{\pm}$  and (iii)  $E_{PV} \sim E_{\pm}$  in several molecules. The ultra-small, handed-signed  $E_{PV}$  of rigid enantiomers cannot interfere with  $E_{\pm}$  value. Quack tabulated  $E_{PV}$  and  $E_{\pm}$  values of twenty non-rigid rotamers and showed that the sign of  $E_{PV}$  in non-rigid XZ–ZX type rotamers (X = H, D, T, Cl and Z = O, S, Se, Te) alters, depending on the rotatable angles and also that in XO–OX molecules (X = H, D, T, Cl),  $E_{PV} \ll E_{\pm}$ . [49] Although the  $E_{PV}$  and  $E_{\pm}$  values are susceptible to the nature of the rotamers, the former changes by a factor of  $10^5$  while the latter changes by a factor of  $10^{25}$ . This estimation implies an increase in rotational barrier height of XZ–ZX rotamers. Actually, among the XZ–ZX rotamers, only  $T_2S_2$  satisfies the  $E_{PV} \sim E_{\pm}$  condition [46]. The rotational barrier of HO–OH is rather high: around  $7.5 \text{ kcal mol}^{-1}$ . To interfere efficiently between  $E_{PV}$  and  $E_{\pm}$ , the  $E_{PV} \sim E_{\pm}$  criterion using non-radioactive substances should be designed experimentally because radioactive T is not available.

So far, several experimental groups reported the validity of the MSB hypothesis by seeking subtle differences in physical and optical properties between enantiomeric species; for example, high-resolution vibrational and ro-vibrational spectroscopy of rigid chiral organic and inorganic molecules in a vacuum [52,53], spontaneous crystallization of coordination compounds including heavy metal ions [54], single crystals of D-/L-amino acids [55], helix-coil transition characteristics of oligo-D-/L-amino acids [56],  $\alpha$ -helix  $\rightarrow$   $3_{10}$ -helix transition characteristics of poly-(D-/L)-glutamic acids [57],  $7_3$ -helix  $\rightarrow$   $7_3$ -helix transitions characteristics of Si–Si bond polymers [58–60] and more recently, anomalies in thermal and NMR relaxation properties of metal-organic frameworks [61,62]. The possibility of detecting a *D-L* preference between enantiomers under thermal equilibrium conditions is beyond doubt, yet definitive experimental answers have remained elusive because of the stringent requirements for very specific mirror-image molecules satisfying 100% *ee* purity in the ground ( $S_0$ ) state.

By learning from successful  $\beta^{\pm}$ -decay and *APV* radiation experiments [6–8,20,22], we postulated that non-rigid  $\pi$ -conjugated luminophores in symmetrical DW/multiple-wells (MW) with lower  $E_b$  values in the lowest photoexcited ( $S_1$ ) state at the allowed transitions allow for possible detection the *MPV* effect. Aiming at verifying our idea, we tested several non-rigid luminophores including oligofluorenes (up to seven repeating units), linear and cyclic oligo-*p*-arylenes (up to twelve repeating units),  $C_2$ -symmetrical binaphthyls and fused aromatics (three acenes and pyrenes) carrying rotatable side groups. To control experimentally the tunneling barrier  $E_b$  in these luminophoric systems at the  $S_1/S_0$  states, we chose various achiral liquids, including linear-/branched alkanes, linear-/branched alkanols, haloalkanes, linear-/cyclic-ethers and others. The viscosity [ $\eta$  in *cP*] is broadly tunable, ranging from 0.21 to 71.0 at 20–25 °C [63–65]. The solvent viscosity plays a role in the *continuous* control of the  $E_b$  value of the tunneling potential surface of non-rigid molecules [48,49,51] at the  $S_1/S_0$  states, enabling fulfillment the  $E_{\pm} \sim E_{pv}$  criteria.

Without exception, all the non-rigid fluorophores showed negative-sign CPL signals in the UV-visible region, suggesting that energetically inequivalent, non-mirror image structures at the  $S_1$  state are temporarily generated. For comparison, four fused aromatic fluorophores did not show clear CPL signals. The non-rigid fluorophores boosted progressively but *discontinuously* in a quantized behavior while keeping negative-sign CPL spectra in the range of  $g_{\text{lum}} = -0.2 \times 10^{-3}$  to  $-2.0 \times 10^{-3}$  in response to the viscosity of the liquids. In a series of oligofluorenes, the  $g_{\text{lum}}$  value at zero viscosity was extrapolated to  $-0.8 \times 10^{-3}$  at 420 nm when more than 7 fluorene rings are fused. This non-zero  $g_{\text{lum}}$  value suggested that the photoexcited oligofluorenes emit (-)-sign CPL signals in a vacuum, originating from the hypothesized *PV-WNC* coupled with the ring-current of the aromatics under conditions of zero magnetic field.

## 2. Results

The handed electron–nuclei interactions force enables CPL-silent/CD-silent molecules into CPL-active/CD-active ones at the  $S_1/S_0$  states. Although heavier atoms, like Si, Ge, Sn, Pb, Se, Te, Fe, Ru, Re, W, Os and U, are involved in the luminophores,  $E_{\text{PV}}$  may be boosted by the  $V_{\text{SO}} (\propto Z^2)$  law. However, luminescent species might be phosphorescent with an inefficient quantum yield (PLQY, typically, <0.01) and is difficult to detect as CPL/PL signals in an excellent S/N ratio. Therefore, we focused on fluorophores comprising lighter atoms because of an efficient PLQY, typically, 0.1–0.9. The values of the spin-orbit interaction ( $\zeta$ ) for lighter atoms (C, N, O, F, S) are considerably large  $\zeta$  values such that 0.1, 0.2, 0.4, 0.7, 1.0 kcal mol<sup>-1</sup>, respectively [66]. These fluorophores are utilized as laser dyes, highly emissive dyes, biomarkers and scintillators. If huge numbers ( $>10^{10}$ – $10^{16}$ ) of the non-rigid enantiomeric fluorophores in a cuvette are photoexcited macroscopically and simultaneously, the ultra-tiny *ee* or faint  $E_{\text{PV}}$  of an isolated molecule may be greatly boosted to the detectable level, according to the linear amplification model [28] and/or the highly cooperative phase transition models at the far-from, non-equilibrium, open-flow  $S_1$  state [41].

Alternatively, when Kasha's rule in Jablonski diagram is considered [66,67], fluorescence should occur from only 'the lowest vibrionic  $S_1$  state' during the courses of non-radiative, ro-vibrational/translational processes even if the luminophores are photoexcited at  $S_2$  and higher  $S_n$  states. Possible radiation scenarios are classified to four cases.

The inherently rigid achiral luminophores do not emit CPL signals and do not reveal CD signals.

The rigid chiral luminophores involve point chirality and/or axial chirality, that act as parity-conserving strong chiral electromagnetic (*EM*) force at the  $S_1/S_0$  states. The rigid chiral luminophores at the  $S_1$  state adopt the similar geometry of the corresponding  $S_0$  state due to minimal reorganization processes in a highly symmetrical DW, sign and magnitude of CPL between enantiomers should be mirror-image.

When non-rigid CD-silent enantiomers in a symmetrical DW at the  $S_1$  state coexist equally, the enantiomers may rapidly oscillate between *L*- and *R*-states with time at the  $S_1$  state, resulting in time-averaged null-CPL signals.

If the non-rigid enantiomers turn into a dissymmetrical DW at the  $S_1$  state by quitting the oscillating fashion, only (+)- or (-)-sign CPL signals are detectable *via* noticeable handed rotational and/or flip-flop motions.

### 2.1. Rigid Achiral Planar $\pi$ -Conjugated Luminophores

Firstly, to ensure neutrality in CPL- and CD-signals of achiral  $D_{2h}$  symmetrical  $\pi$ -conjugated aromatic compounds that involve naphthalene (1), anthracene (2), tetracene (3) and pyrene (4) (Chart 1) without substituents in the  $S_1$  and  $S_0$  states, we measured the CPL- and CD-spectra in a low viscosity methanol ( $[\eta] = 0.55 \text{ cP}$ ) and several solvents. Although artifact-free precision measurements are serious concerns of single 50-KHz PEM CPL and CD spectrometers [68–70], no detectable CPL- and CD-signals at the corresponding PL and UV-visible spectra were confirmed for 1 (Figure 1a,b), 2 (Figure 1c,d),

3 (Figure 1e,f) and 4 (Figure 1g,h). Our CPL (JASCO CPL-200) and CD (JASCO J-820) spectrometers guaranteed the null CD and CPL signals of 1–4.

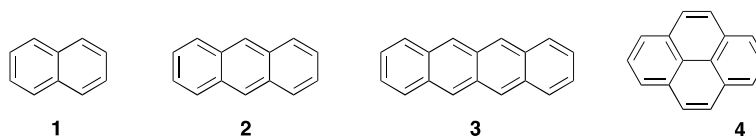


**Chart 1.** Chemical structures of  $D_{2h}$ -symmetrical fused aromatics: naphthalene (1), anthracene (2), tetracene (3) and pyrene (4).

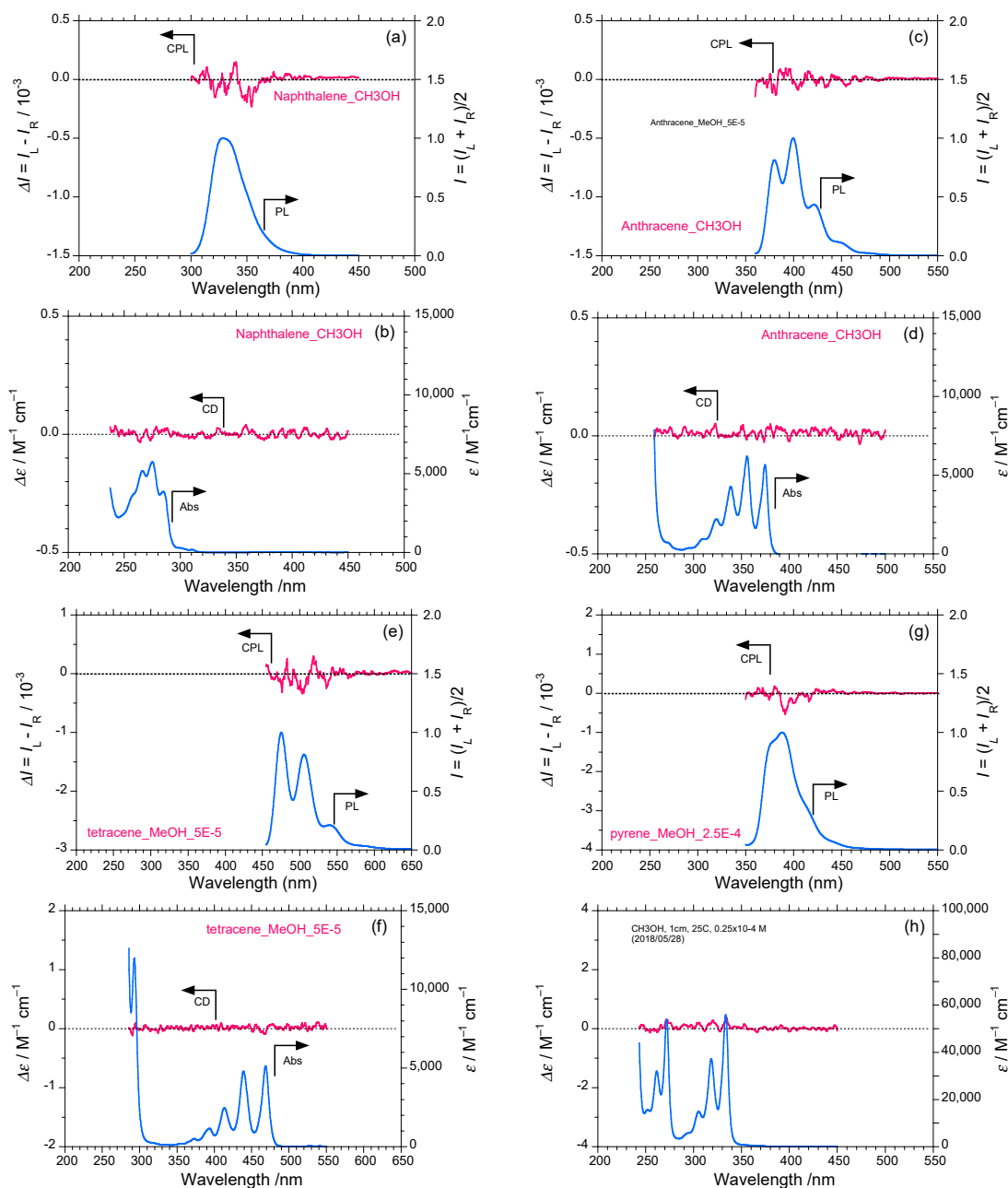


**Figure 1.** CPL/PL and CD/UV-vis spectra of  $D_{2h}$ -symmetrical fused aromatics in methanol at room temperature. (a) CPL/PL spectra excited at 270 nm and (b) CD/UV-vis spectra of 1. (c) CPL/PL spectra excited at 310 nm and (d) CD/UV-vis spectra of 2. (e) CPL/PL spectra excited at 420 nm and (f) CD/UV-vis spectra of 3. (g) CPL/PL spectra excited at 320 nm and (h) CD/UV-vis spectra of 4. Measurement conditions: path length: 10 mm, cylindrical cuvette, conc.:  $(2.5\text{--}5.0) \times 10^{-5}$  M.

## 2.2. Rigid Planar $\pi$ -Conjugated Luminophores Bearing Phenyl and Phenylethynyl Rotors

On the other hand, pseudo- $D_{2h}$  symmetrical frameworks bearing rotatable phenyl groups and phenylethynyl groups (5–9, Chart 2) showed (–)-sign CPL signals at the corresponding PL bands in methanol and other solvents (Figure 2 and Figure S1 Supplementary Materials (SM)). Molecules 5 and 6, corresponding to 1 bearing two phenyl groups and two phenylethynyl groups in the 9,10-positions, respectively, showed weak vibronic CPL bands in methanol (Figure 2a,e). Evidently, the CPL signals of 5 and 6 are significantly boosted in the more viscous solvents *n*-undecanol (16.95 *cP*) and 1,4-butanediol (71.0 *cP*) (Figure 2b,f and Figure S1a in SM)).

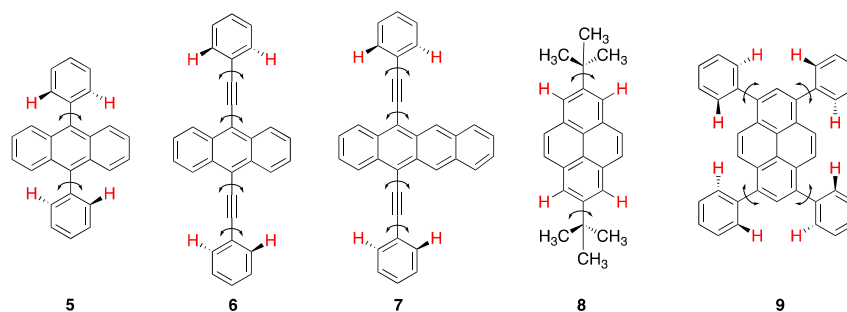


**Chart 2.** Chemical structures of fused aromatics bearing rotatable substituents: 9,10-diphenylanthracene (5), 9,10-bis(phenylethynyl)anthracene (6), 5,12-bis(phenylethynyl)-tetracene (7), 2,7-di-*tert*-butylpyrene (8) and 1,3,6,8-tetraphenylpyrene (9).

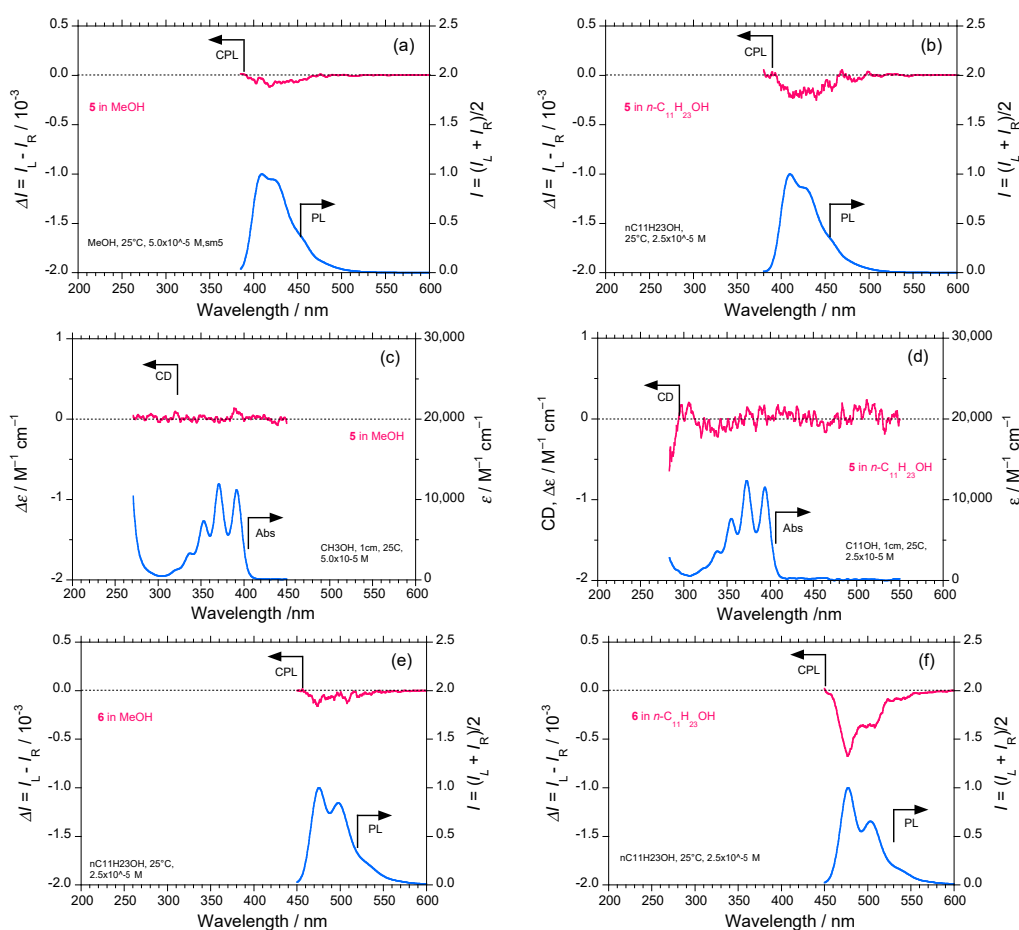


**Figure 2.** Cont.

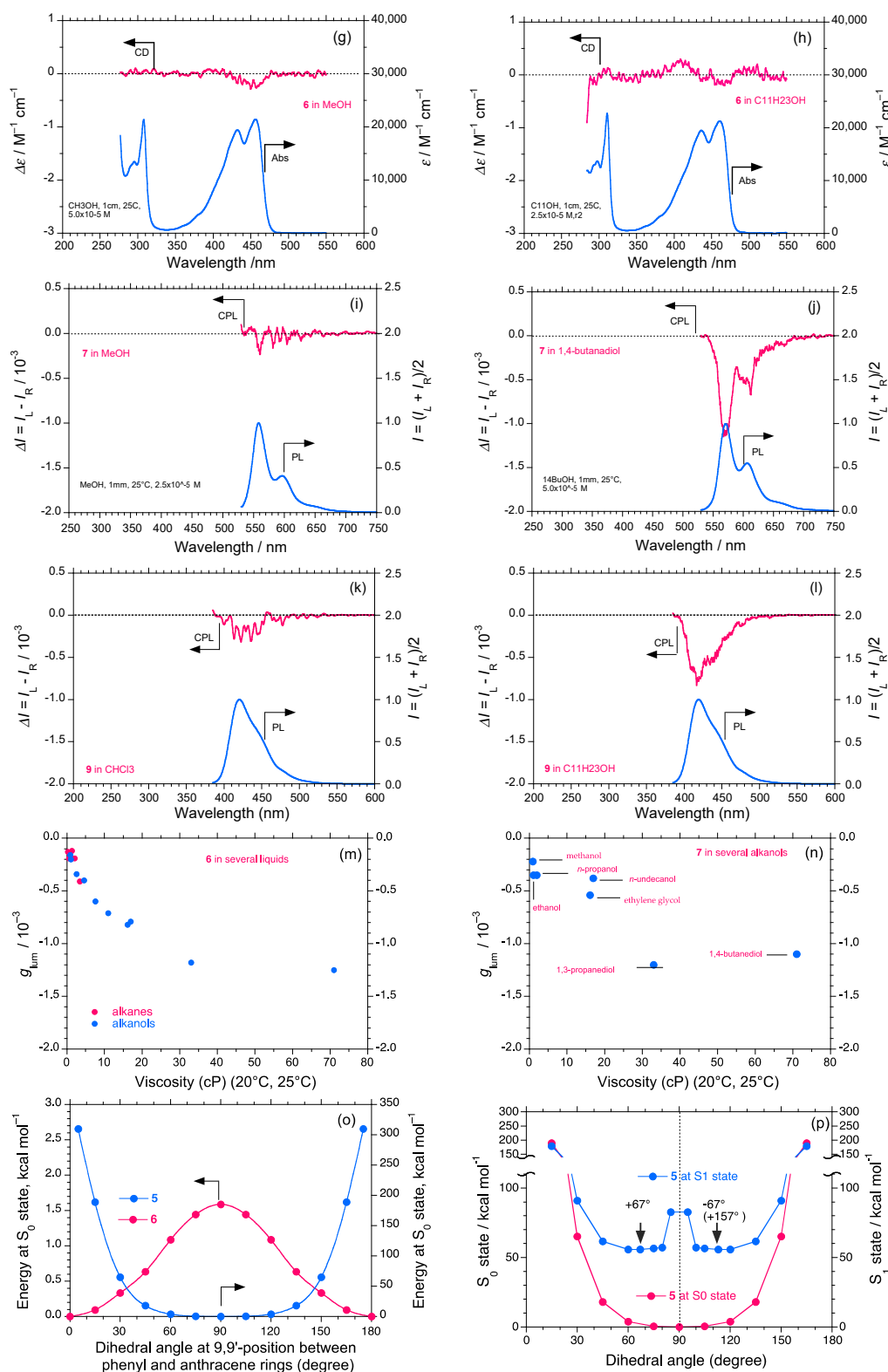


**Figure 2.** CPL/PL and CD/UV-vis spectral characteristics of pseudo- $D_{2h}$ -symmetrical fused aromatics carrying multiple rotatable substituents in various liquids at room temperature. (a) CPL/PL spectra of 5 excited at 355 nm and (c) CD/UV-vis spectra in methanol. (b) CPL/PL spectra of 5 excited at 355 nm and (d) CD/UV-vis spectra in *n*-undecanol. (e) CPL/PL spectra of 6 excited at 420 nm and (g) CD/UV-vis spectra in methanol. (f) CPL/PL spectra of 6 excited at 420 nm and (h) CD/UV-vis

spectra *n*-undecanol. CPL/PL spectra of **7** excited at 500 nm in (i) methanol and (j) 1,4-butanediol. CPL/PL spectra of **9** excited at 355 nm in (k) chloroform and (l) *n*-undecanol. (m) The  $g_{lum}$  value (in  $10^{-3}$ ) at 475 nm of **6** as a function of viscosity of achiral liquids consisting of alkanes and alkanols; *n*-pentane,  $-0.13$ , *n*-octane  $-0.19$ , *n*-decane  $-0.17$ , *n*-dodecane  $-0.12$ , *n*-tetradecane  $-0.19$ , *n*-hexadecane  $-0.41$ , methanol  $-0.16$ , ethanol  $-0.20$ , *n*-butanol  $-0.34$ , *n*-hexanol  $-0.40$ , *n*-octanol  $-0.60$ , *n*-decanol  $-0.71$ , *n*-undecanol  $-0.79$ , ethylene glycol  $-0.82$ , 1,3-propanediol  $-1.18$ , 1,4-butanediol  $-1.25$ . (n) The  $g_{lum}$  value (in  $10^{-3}$ ) of **7** as a function of viscosity of achiral liquids. Measurement conditions: path length: 10 mm, cylindrical cuvette, conc.:  $(2.5-5.0) \times 10^{-5}$  M at room temperature. (o) Energy of **5** and **6** optimized at  $S_0$  state as a function of dihedral angle of two phenyl moieties at 9,10-position of anthracene. (p) Energy of **6** optimized at  $S_0$  and  $S_1$  states as a function of dihedral angle of two phenyl moieties at 9,10-positions of anthracene. These calculations were performed by DFT method (B3LYP functional with 6-31Gd basis set).

It is notable that the CPL signals of **6** in *n*-undecanol are more obvious than those of **5** in *n*-undecanol, though the rotational barrier of the phenylethynyl group should be smaller than that of phenyl group. We observed a very weakly (-)-sign CD signal for **6** in methanol on the order of  $g_{abs} \sim -1 \times 10^{-5}$  at 456 nm (Figure 2g), while **6** in *n*-undecanol a clear CD signal is not obvious (Figure 2h). Subtle alteration of the phenyl and phenylethynyl groups in the peripheral 9,10-positions of **2** may affect these CPL and/or CD characteristics. Similarly, molecule **7**, which is a derivative of **3** carrying phenylethynyl groups in 5,12-positions, showed clearly vibronic CPL signals at the corresponding PL bands in 1,4-butanediol (Figure 2j), although the signals in methanol were very weak (Figure 2i). The CD signal of **7** in methanol is not obvious (Figure S2b in SM).

These noticeable solvent dependent CPL characteristics led us to plot the  $g_{lum}$  values of **6** and **7** as a function of the viscosity of *n*-alkanes and alkanols (Figure 2m,n). When  $[\eta] > 30$  cP, the  $g_{lum}$  values of **6** and **7** progressively approach to  $-1.2 \times 10^{-3}$ . These  $g_{lum}$ -viscosity relationships might be the key in order to discuss the mirror symmetry breaking of semi-rigid and non-rigid luminophores at the  $S_1$  state.

To further verify the substituent effects, we tested the CPL/PL spectral characteristics of two pyrene derivatives (**9**) carrying four phenyl groups in the 1,3,6,8-positions of **4** and for comparison, **8** carrying two *tert*-butyl groups in the 2,7-positions of **4**. Similar to the case of **5**, molecule **9** in *n*-undecanol clearly revealed (-)-sign CPL signals, which were only weakly evident in chloroform (Figure 2k,l). Molecule **8** in *n*-C<sub>6</sub>H<sub>14</sub> ( $[\eta] = 0.30$  cP) revealed derivative-like vibronic CPL signals (Figure S1c in SM). The steric repulsion between multiple protons on the phenyl rings in **5** and **9** (marked in red, Chart 2) and multiple protons in their fused aromatic frameworks may efficiently induce certain handed twisted conformations at the  $S_1$  states. CD signals of **8** in methanol and **9** in methanol and *n*-undecanol are not obvious (Figure S1d-f in SM). Further CD measurements confirmed no detectable signals for **8** or **9** in the range 400–500 nm in ethanol, *n*-propanol, 1,3-propanediol or 1,4-butanediol (Figure S1f in SM).

To test the degree of steric repulsion, Gaussian09 calculations (DFT, B3LYP functional at 6-31G (d, p) level) of **5** and **6** at the  $S_0$  and  $S_1$  states were employed as a function of the dihedral angle ( $\theta$ ) between the anthracene and phenyl rings. Molecule **5** prefers a perpendicular geometry at  $\theta = 90^\circ$ , while, **6**, conversely, prefers a coplanar geometry with  $\theta = 0^\circ/180^\circ$  (Figure 2o). However, **5** at the  $S_1$  state has two global minima, at  $+67^\circ$  and  $+157^\circ$  ( $-67^\circ$ ), indicating that the anthracene and phenyl rings prefer a tilted aspect with left- and right-twisted geometries (Figure 2p). However, **6** at the  $S_1$  state, prefers a coplanar geometry with  $\theta = 0^\circ/180^\circ$  (not shown, similar to Figure 2o). If the two twists exist equally at the  $S_1$  state, CPL signals are not detectable. If the two twists exist due to energetical inequality at the  $S_1$  state, CPL signals are detectable.

### 2.3. Rigid and Non-Rigid Chiral Luminophores

To confirm whether rigid chiral luminophores at the  $S_0$  and  $S_1$  states reveal mirror image CD and CPL spectra in UV-visible regions, we tested enantiomers of C<sub>1</sub>-symmetrical camphor (*D*-10 and *L*-10) and three kinds of pseudo-C<sub>2</sub>-symmetrical BINOL derivatives with axial chirality (*R*-11 and *S*-11,



*R*-12 and *S*-12 and *R*-13 and *S*-13) (Chart 3). Camphor is a representative chiral bicyclic ketone and often used as a chiroptical standard for CPL, CD and VCD spectrometers as it is a naturally occurring chiral substance with a high enantiopurity [70,71]. Also, *R*-11 and *S*-11 are known to emit CPL signals with equal magnitude and the opposite sign as a result of the lack of rotational freedom between the two naphthyl rings restricted by hydrogen phosphophate linkage [72–75]. However, it is noting that *R*-12/*S*-12 and *R*-13/*S*-13 retain rotational freedom at the 1,1'-axial positions between the two naphthyl rings [72,74].

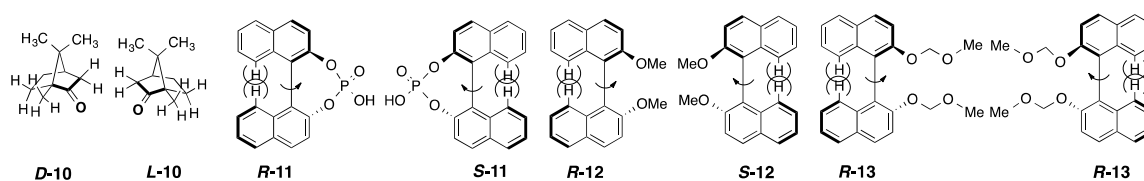


**Chart 3.** Chemical structures of rigid  $C_1$ -symmetric aliphatic ketone and semi-rigid pseudo- $C_2$ -symmetric binaphthyl derivatives: *D*- and *L*-camphor (**10**), (*S*)- and (*R*)-1,1'-binaphthyl-2,2'-diyl hydrogen phosphate (**11**), (*S*)- and (*R*)-2,2'-dimethoxy-1,1'-binaphthyl (**12**) and (*S*)- and (*R*)-2,2'-bis(methoxymethoxy)-1,1'-binaphthyl (**13**).

The rigid luminophores, *D*-10/*L*-10, in cyclohexane revealed ideal mirror image profiles of vibronic CD and non-vibronic bisignate CPL spectral line shapes with opposite sign and equal magnitude (Figure 3a,c) [70,71]. Similarly, *R*-11/*S*-11 in lower viscosity solvents (*n*-pentane (0.21 *cP*), methanol (0.55 *cP*) and chloroform (0.55 *cP*)) revealed mirror image vibronic CD and vibronic CPL spectral profiles with opposite sign and equal magnitude (Figure 3b,d and Figure S2a,b in SM). Thus, the CPL and CD spectrometers afford reliable evidence for the measurement of ideal mirror-image CD and CPL spectral sets between enantiomers of rigid chiral emitters in lower viscosity solvents at the  $S_1$  and  $S_0$  states. However, *R*-11/*S*-11 in higher viscosity solvents (ethylene glycol (16.1 *cP*), 1,3-propanediol (33.0 *cP*) and 1,4-butanediol (71.0 *cP*)) [64] revealed non-mirror image CPL spectra (Figure 3e,f,h). As the viscosity increased from 16 to 71 *cP*, the absolute magnitude of the CPL of (*R*)-11 at ~350 nm weakens. Moreover, CPL  $\lambda_{\text{ext}}$  wavelengths (pink and sky-blue bars) between (*R*)- and (*S*)-11 progressively tended to differ from each other. Noticeably, the corresponding CPL spectra between (*R*)- and (*S*)-11 in 1,4-butanediol differ significantly from each other, indicating the absence of enantiomers in the  $S_1$  state (green box in Figure 3h). Also, the corresponding UV-visible spectra of (*R*)- and (*S*)-11 in ethylene glycol differ from each other, indicating the absence of enantiomers in the  $S_0$  state (green box in Figure 3g).

Similarly, although *R*-12/*S*-12 in lower viscosity solvents such as *p*-dioxane (1.10 *cP*), chloroform, *n*-pentane and methanol showed CPL spectra with near mirror image profiles but with subtle differences associated with vibronic bands (Figure S2c–f in SM), *R*-12/*S*-12 in ethanol (1.09 *cP*), *n*-propanol (1.96 *cP*) and ethylene glycol reveals the absence of mirror image CPL spectra (Figure 3i–k) and in 1,4-butanediol (71 *cP*) showed typically (–)-sign CPL spectra associated with different wavelengths (Figure 3l), whilst the CPL  $\lambda_{\text{ext}}$  wavelengths (pink and sky blue bars) between (*R*)-11 and (*S*)-11 differ from each other (Figure 3l). These non-mirror image CPL spectral characteristics can be recognized from the inconsistent PL spectral profiles between *R*-12 and *S*-12 in ethanol, ethylene glycol, 1,3-propanediol and 1,4-butanediol (green boxes in Figure 3i,k,l and Figure S2g in SM).

On the other hand, *R*-12 and *S*-12 at the  $S_0$  state reveal ideal mirror image CD spectra in these solvents, indicating adoption of mirror-image geometries regardless of the solvents (Figure S3h–j) in SM). It is noteworthy that the longest wavelength CD Cotton effects of *R*-11 and *S*-11 are the opposite of the corresponding *R*-12 and *S*-12 (Figure 3d vs. Figure S3h–j in SM). This apparent inversion phenomenon is likely to arise from alteration in dihedral angle between the two naphthyl rings at the  $S_1$  state [72–75]. Actually, *R*-12 showed a (+)-sign CPL spectrum, while *R*-11 showed a (–)-sign CPL spectrum. *S*-12 in 1,4-butanediol favored a (–)-sign CPL spectrum. Similarly, although *R*-13 and *S*-13 at

the  $S_0$  state had nearly ideal mirror image CD spectra (Figure 3n), even in *n*-pentane, they no longer had mirror image CPL spectra (Figure 3m).

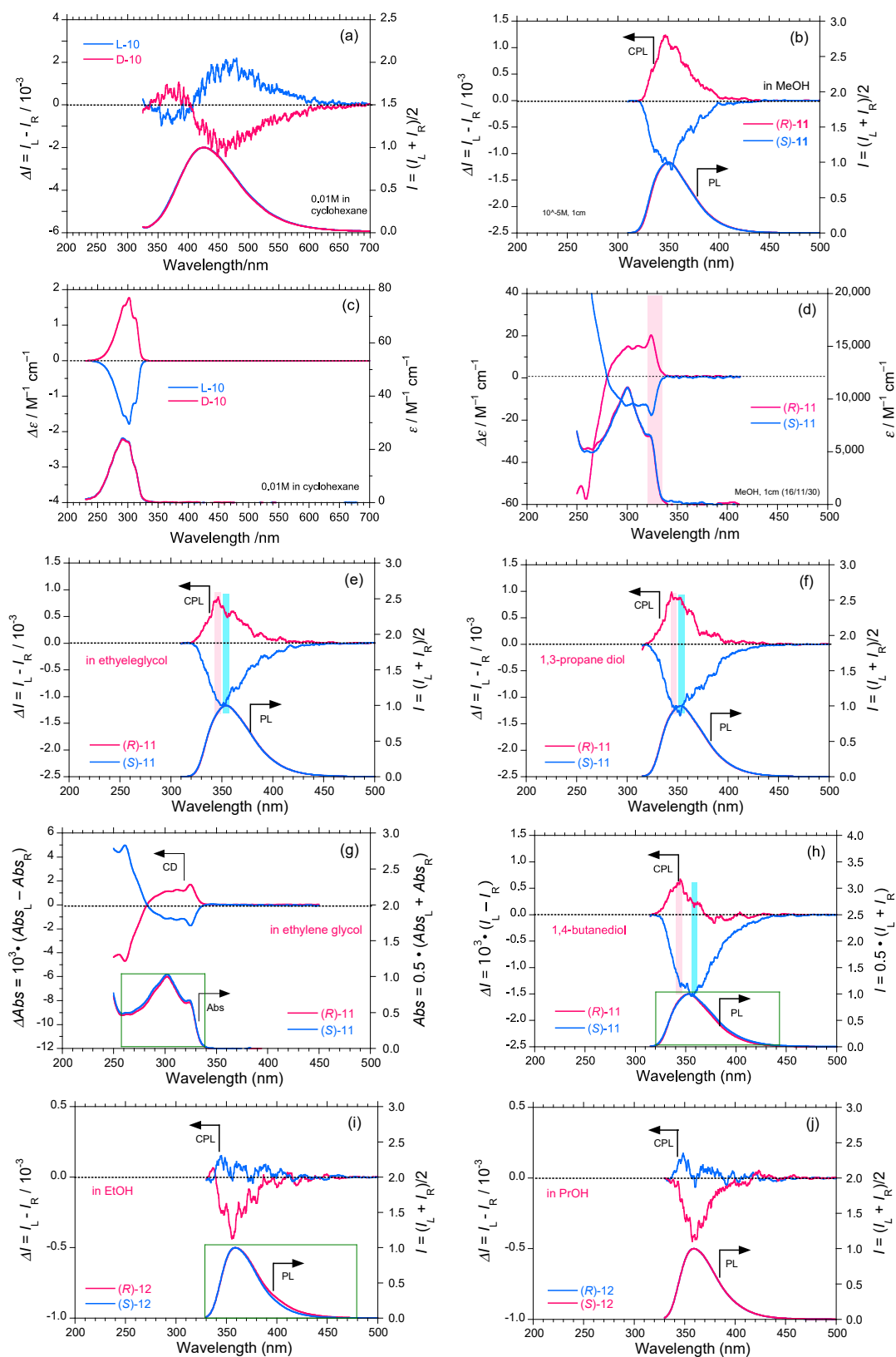
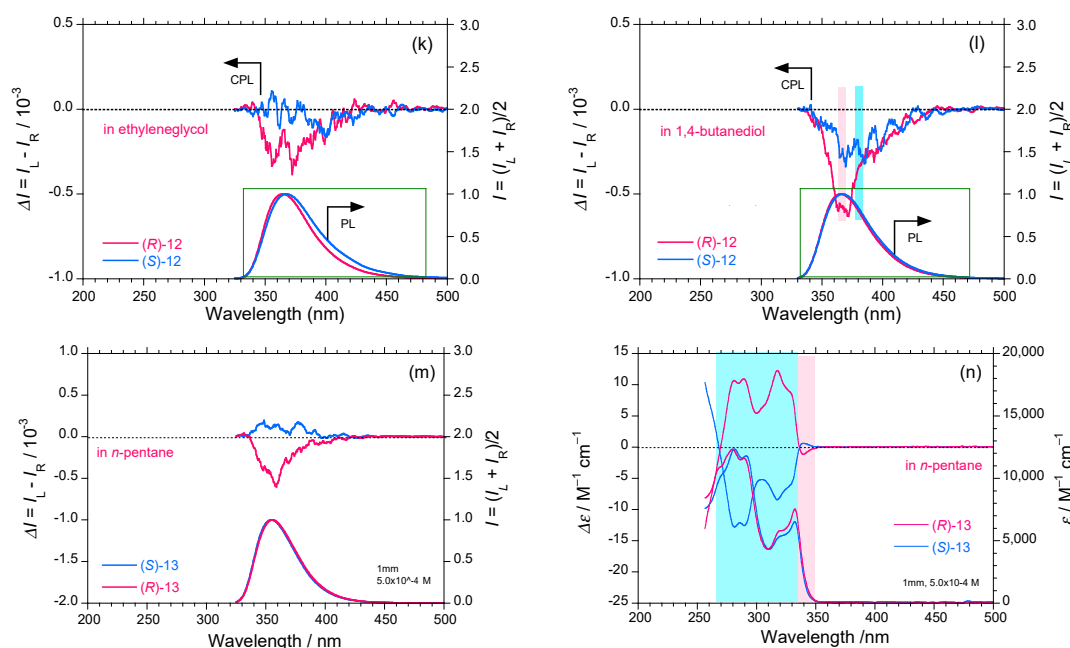


Figure 3. Cont.



**Figure 3.** CD/UV-vis and CPL/PL spectra of rigid bicyclic camphor, rigid binaphthol derivatives and semirigid binaphthol derivatives allowing pivotal motion in various solvents at room temperature (path length: 10 mm, cylindrical cuvette,  $[conc]_0 = (2-5) \times 10^{-4}$  M): (a) CPL/PL spectra of *D*-10 and *L*-10 excited at 295 nm and (c) CD/UV-vis spectra in cyclohexane; (b) CPL/PL spectra of *R*-11 and *S*-11 excited at 290 nm and (d) CD/UV-vis spectra in methanol; CPL/PL spectra of *R*-11 and *S*-11 excited at 290 nm (e) in ethylene glycol, (f) in 1,3-propanediol and (h) in 1,4-butanediol; (g) CD/UV-vis spectra of *R*-11 and *S*-11 in ethylene glycol; CPL/PL spectra of *R*-12 and *S*-12 excited at 295 nm (i) in ethanol, (j) in *n*-propanol, (k) in ethylene glycol and (l) in 1,4-butanediol; (m) CPL/PL spectra *R*-13 and *S*-13 excited at 295 nm and (n) CD/UV-vis spectra in *n*-pentane.

Thus, semirigid chiral BINOL derivatives, *R*-11/*S*-11 and non-rigid chiral BINOL derivatives, *R*-12/*S*-12 and *R*-13/*S*-13 at the  $S_1$  states showed no mirror image relationship between their CPL spectra, even though mirror image CD spectra were observed at the  $S_0$  states. This anomaly should arise from rotational freedom at the  $S_1$  state between the two naphthyl rings regardless of solvent viscosity, similar to the cases of 5, 6, 7 and 9.

#### 2.4. Linear and Cyclic Oligo-*p*-Phenyl Derivatives without and with Rotatable Alkyl Substituents

Linear and recently reported cyclic oligo-*p*-phenyls with and without methyl and *t*-butyl substituents are among the simplest extended  $\pi$ -electron systems (Chart 4). Linear oligo-*p*-phenyls have been utilized as luminophores in dye lasers and scintillators in near-UV and visible region for many years [76–78] due to their photochemically and thermally robust features. Although unsubstituted oligo-*p*-phenyls longer than five or six repeating units have limited solubility, *p*-dioxane is commonly used as a solvent for reasons not fully understood by the authors. In contrast, methyl- and *t*-butyl-substituted oligo-*p*-phenyls show excellent solubility in common organic solvents. Nevertheless, unsubstituted cyclic-*p*-phenyls recently synthesized are also readily soluble in common organic solvents, permitting their utilization as luminophores in which the emission band is controllable by ring number [79,80]. Due to inherent repulsions in closely approaching Ar-*H*/*H*-Ar and/or Ar-CH<sub>2</sub>-*H*/*H*-Ar pairs, these linear and cyclic oligo-*p*-phenyls can twist in left or right directions cooperatively.

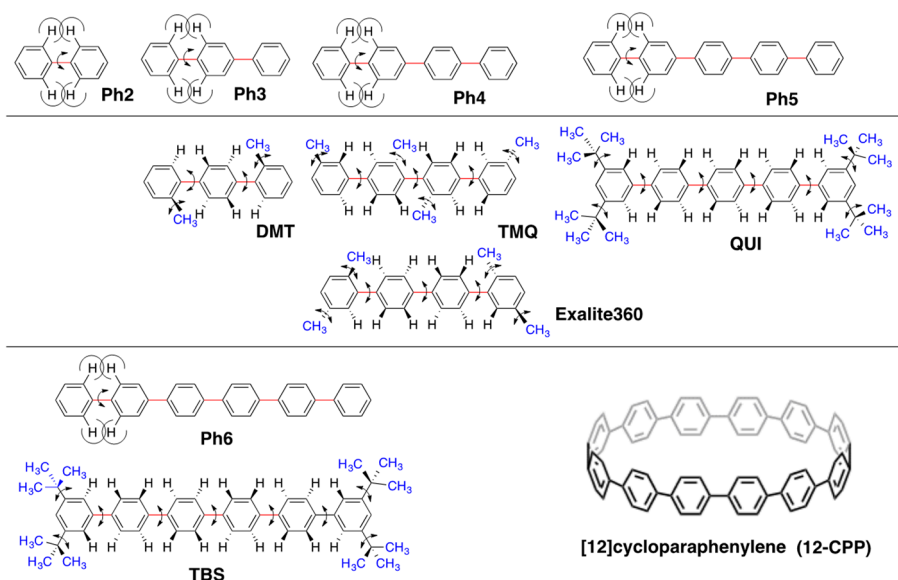


**Chart 4.** Chemical structures of non-rigid linear and cyclic oligo-*p*-phenyls: biphenyl (Ph2), *p*-terphenyl (Ph3), *p*-quaterphenyl (Ph4), *p*-quinquephenyl (Ph5), *p*-sexiphenyl (Ph6), 2,2''-dimethyl-1,1':4'1''-terphenyl (DMT), 2'',3,3',3'''-tetramethyl-1,1':4'1'':4'',1''''-quaterphenyl (TMQ), 2,5,2''',5''''-tetramethyl-*p*-quaterphenyl (Exalite360), 3,5,3''',5''''-tetra-*t*-butyl-*p*-quinquephenyl (QUI), 3,5,3''',5''''-tetra-*t*-butyl-*p*-sexiphenyl (TBS) and [12] cycloparaphenylene (12-CPP).

CPL/PL spectra of biphenyl (Ph2), *p*-terphenyl (Ph3), *p*-quaterphenyl (Ph4) and *p*-quinquephenyl (Ph5), in *p*-dioxane and [12] cyclo-*p*-phenylene (12-CPP) in *p*-dioxane and squalene are depicted in Figure 4a–f. Except for Ph2, CPL signals of Ph3, Ph4, Ph5 and 12-CPP in *p*-dioxane are obvious and their  $g_{\text{lum}}$  values range from  $-0.15 \times 10^{-3}$  and  $-0.25 \times 10^{-3}$ . Although 12-CPP in the moderately viscous solvent *n*-hexadecane [3.47 *cP*] has weaker  $g_{\text{lum}} = -0.16 \times 10^{-3}$  at 425 nm (Figure S3c in SM), 12-CPP in squalene (29.5 *cP*) is greatly increased to  $g_{\text{lum}} = -0.6 \times 10^{-3}$  at 425 nm (Figure 4i) and CPL signals are obvious in chloroform, *n*-pentane and *n*-hexadecane (Figure S3a,b,d) in SM.

The  $g_{\text{lum}}$  value at  $\lambda_{\text{ext}}$  of Ph2, Ph3, Ph4, Ph5 and 12-CPP in *p*-dioxane and other solvents as a function of phenyl ring number is plotted in Figure 4g. Additionally, the  $g_{\text{lum}}$  value at  $\lambda_{\text{ext}}$  of 12-CPP as a function of the viscosity of the five solvents is plotted in Figure 4h. Evidently, the  $g_{\text{lum}}$  value of linear, non-rigid and oligo-*p*-phenyls in *p*-dioxane linearly amplifies to  $-0.8 \times 10^{-3}$  when the phenyl ring number increases from 2 to 5, whilst that of semi-rigid 12-CPP decreases and is similar to the value for Ph4. Rotational freedom along C–C bonds between phenyl rings is likely to be crucial. Similarly, the  $g_{\text{lum}}$  value of 12-CPP amplified nonlinearly and leveled off at  $-0.6 \times 10^{-3}$  as the viscosity increased. The viscosity of the solvents, number of phenyl rings and rotational freedom between phenyl rings appear to be crucial. However, the corresponding CD signals at the corresponding UV-vis spectra of Ph2, Ph3, Ph4, Ph5 and 12-CPP in *p*-dioxane are not obvious (Figure S3e–h in SM).

For comparison, we measured the CPL/PL spectra of highly soluble linear oligo-*p*-phenyl derivatives bearing methyl and *tert*-butyl side groups: 2,2''-dimethyl-1,1':4'1''-terphenyl (DMT), 2,5,2''',5''''-tetramethyl-*p*-quaterphenyl (EX360), 2'',3,3',3'''-tetramethyl-1,1':4'1'':4'',1''''-quaterphenyl (TMQ), 3,5,3''',5''''-tetra-*t*-butyl-*p*-quinquephenyl (QUI) and 3,5,3''',5''''-tetra-*t*-butyl-*p*-sexiphenyl (TBS) in *p*-dioxane (Figure 5a–e) and for comparison, their CD/UV-visible spectra in *p*-dioxane are displayed in Figure S4a–e in SM. DMT, EX360, TMQ, QUI and TBS in 1,4-dioxane, though, all exhibited distinct CPL signals at 333 nm, 352 nm, 350 nm, 372 nm and 380 nm, respectively, despite there being no detectable CD signals. The highest  $g_{\text{lum}}$  values for DMT, EX360, TMQ, QUI and TBS in *p*-dioxane were  $-0.08$ ,  $-0.28$ ,  $-0.74$ ,  $-0.93 \times 10^{-3}$  at the 0-0' or 0-1' band, respectively (Figure 5a–e). The highest  $g_{\text{lum}}$  value had a tendency to increase nonlinearly as phenyl ring number (*n*) increased from *n* = 3 to 6 (Figure 5f).

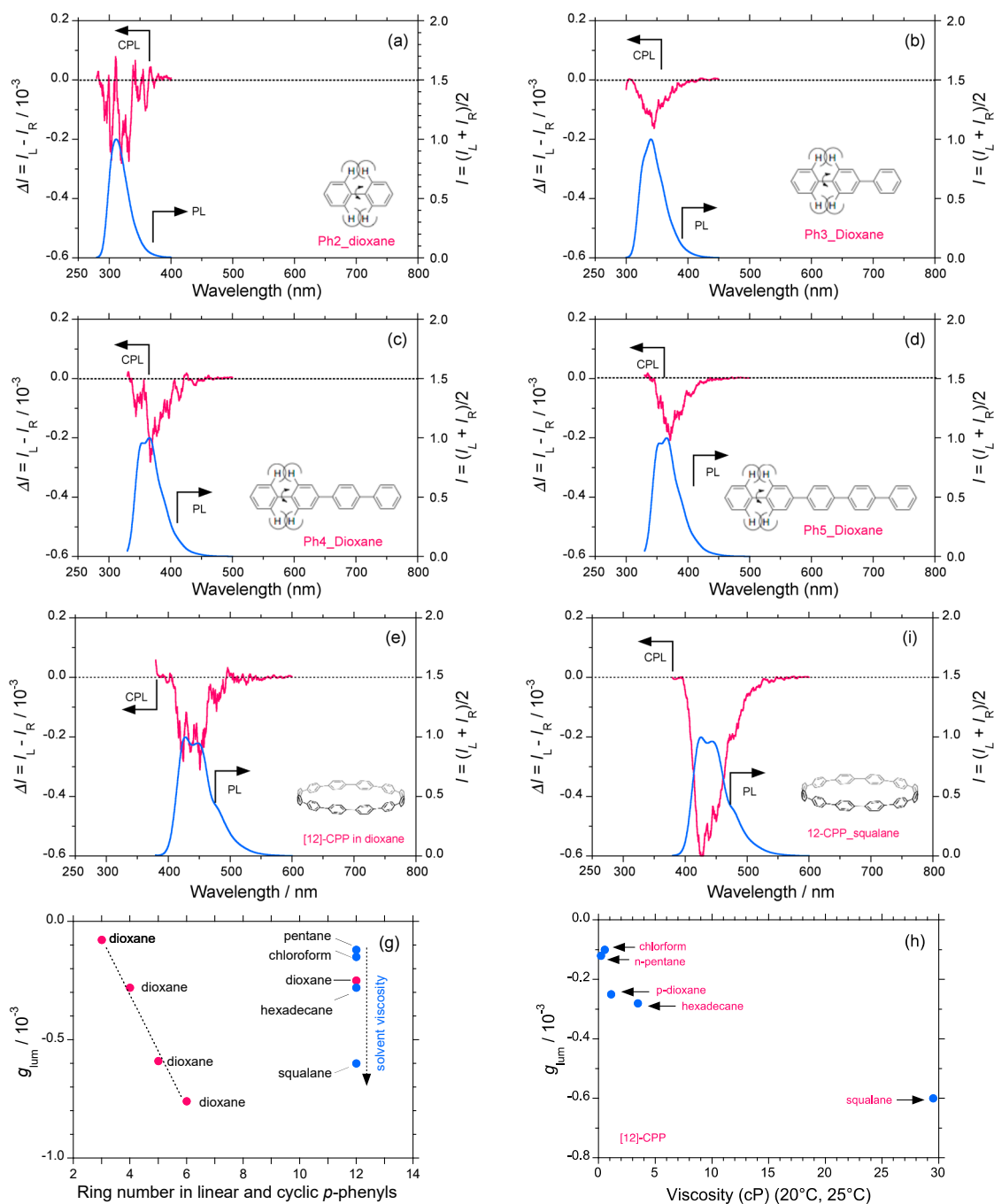


**Figure 4.** CPL/PL spectra of unsubstituted linear and cyclic oligo-*p*-phenyls in several solvents at room temperature (path length: 10 mm, cylindrical cuvette, conc.:  $(0.5\text{--}5) \times 10^{-5}$  M: (a) CPL/PL spectra of Ph2 excited at 250 nm in; (b) CPL/PL spectra of Ph3 excited at 270 nm in *p*-dioxane; (c) CPL/PL spectra of Ph4 excited at 300 nm in *p*-dioxane; (d) CPL/PL spectra of Ph5 excited at 300 nm in *p*-dioxane; (e) CPL/PL spectra of [12]-CPP excited at 350 nm in *p*-dioxane and (f) in squalane. Ph6 was insoluble or scarcely soluble in *p*-dioxane and other solvents; (g) the  $g_{lum}$  value at  $\lambda_{ext}$  of linear and cyclic oligo-*p*-phenyls in *p*-dioxane and other solvents as a function of phenyl ring number; (h) the  $g_{lum}$  value at  $\lambda_{ext}$  of [12]-CPP in five solvents as a function of viscosity (in cP).

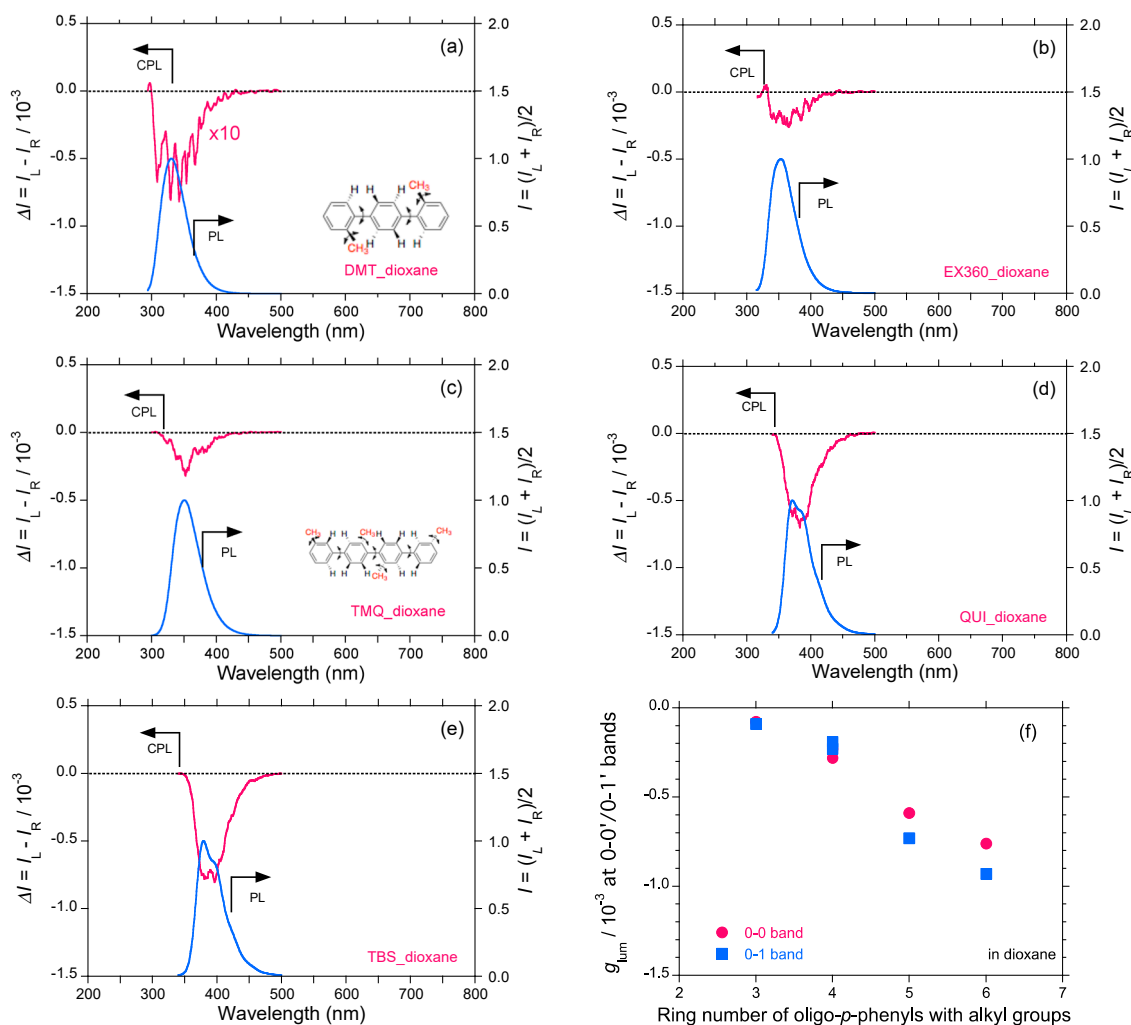


**Figure 5.** CPL/PL spectra of linear oligo-*p*-phenyls bearing methyl and *t*-butyl groups in *p*-dioxane at room temperature (path length: 10 mm, cylindrical cuvette, conc.:  $(2.5\text{--}10) \times 10^{-5}$  M; CPL/PL spectra of (a) DMT excited at 265 nm, (b) Exalite360 excited at 285 nm, (c) TMQ excited at 270 nm, (d) QUI excited at 315 nm and (e) TBS excited at 315 nm; (f) the  $g_{lum}$  value at  $\lambda_{ext}$  of substituted oligo-*p*-phenyls in *p*-dioxane as a function of phenyl ring number in *p*-dioxane.

In the case of viscous *n*-undecanol, these  $g_{lum}$  values increased to DMT  $-0.42 \times 10^{-3}$  at the 0-0' and 0-1' bands (Figure 6a), Exalite 360  $-0.75 \times 10^{-3}$  at the 0-1' band (Figure 6b), TMQ  $-0.42 \times 10^{-3}$  at the 0-1' band (Figure 6c), QUI  $-1.22 \times 10^{-3}$  at the 0-1' band (Figure 6d) and TBS  $-1.28 \times 10^{-3}$  at the 0-1' band (Figure 6e). The highest  $g_{lum}$  value in *n*-undecanol had a tendency to increase nonlinearly as the phenyl ring number (*n*) increased from *n* = 3 to 6 (Figure 6f). Obviously, the  $g_{lum}$  values of QUI and Ex360 in *n*-undecanol at 0-1' band are stronger than those at the 0-0' band, due to the Franck-Condon principle and the great difference in potential energy surfaces and nuclear coordinates between the  $S_1$  and  $S_0$  states. Methyl and *tert*-butyl groups attached to the  $\pi$ -conjugated framework efficiently increased photoexcited state chirality. Efficient coupling between the electronic structure of the  $\pi$ -electron system and the vibration modes of the  $\pi$ -conjugated framework at the  $S_1$  state may be crucial. The highest  $g_{lum}$  value at the 0-1' band in *n*-undecanol tended to increase nonlinearly as the number of Ph rings increased from *n* = 3 to 6, reaching a plateau value of  $-1.3 \times 10^{-3}$  (Figure 6f). Negative-sign CPL signals of EX360 and TBS in viscous ethylene glycol, 1,3-propanediol and 1,4-butanediol and even in *n*-pentane are obvious (Figure S4f–j in SM).

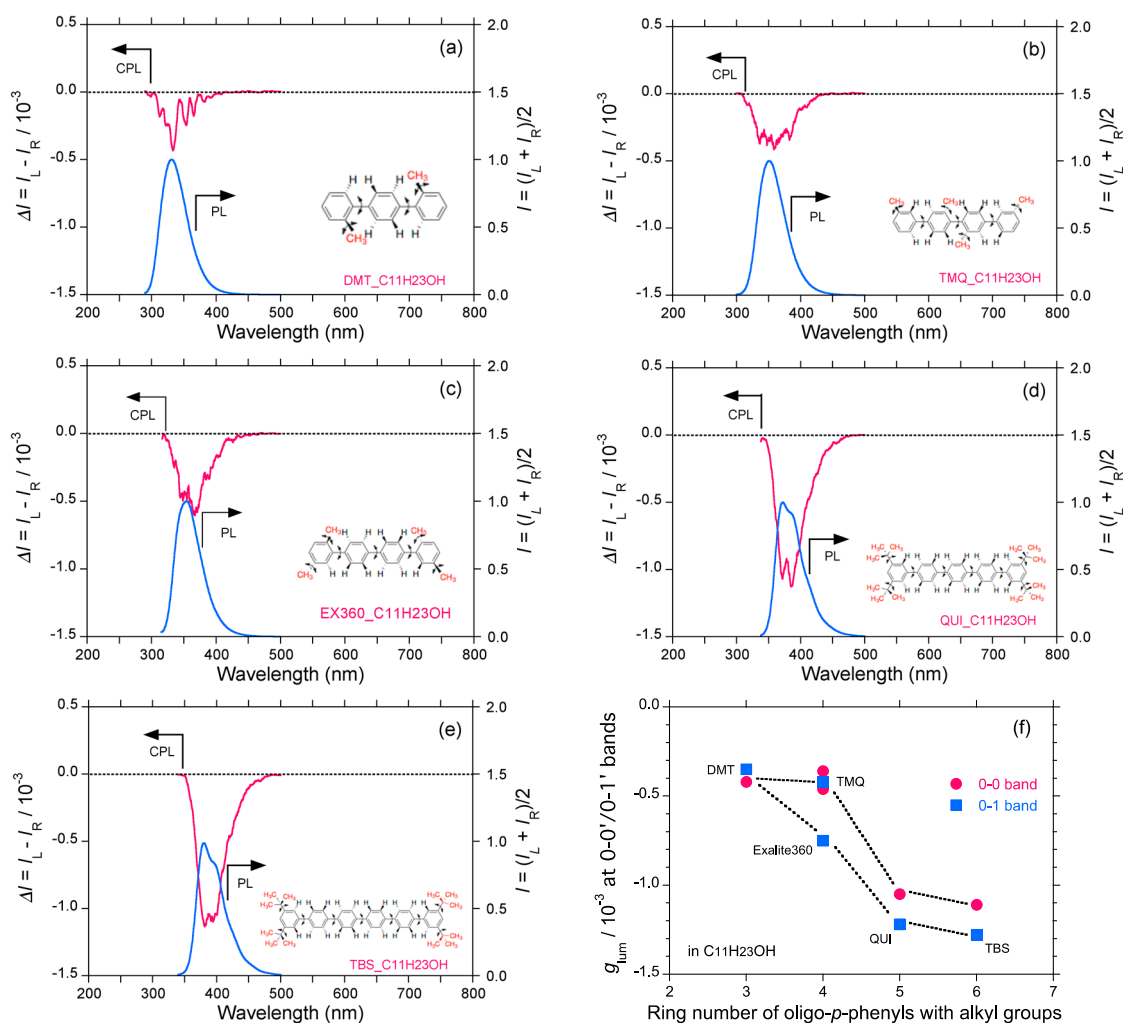


**Figure 6.** CPL/PL spectra of linear oligo-*p*-phenyls carrying methyl and *t*-butyl rotors in *n*-undecanol at room temperature (path length: 10 mm, cylindrical cuvette, conc.:  $(2.5\text{--}10) \times 10^{-5}$  M): (a) CPL/PL spectra of DMT excited at 260 nm, (b) TMQ excited at 270 nm, (c) Exalite360 excited at 280 nm, (d) QUI excited at 310 nm and (e) TBS excited at 315 nm; (f) the  $g_{lum}$  values at the 0-0' and 0-1' bands of  $\lambda_{ext}$  of five oligo-*p*-phenyls with alkyl groups in *n*-undecanol as a function of phenyl ring number.

### 2.5. Chain-Like Non-Rigid Oligofluorene Derivatives Bearing Alkyl Groups

Oligo- and polyfluorenes bearing alkyl chains in the 9,9-positions of the fluorene ring are known to be excellent emitters with a high PLQY of greater than 0.9 at ambient temperature, even in solution [81–83]. The  $C_{2v}$ -symmetrical fluorene ring has V-shaped topology in a planar geometry and can be regarded as a twistable biphenyl derivative (Ph<sub>2</sub>). When two fluorene rings connect to each other at the 2- and 7-positions, even the simplest fluorene dimer adopts four possible geometries: polar  $C_2$ -symmetrical syn-forms with *P*- and *M*-helix senses and less-polar  $C_1$ -symmetrical anti-forms with *P*- and *M*-helix senses. With extension of the fluorene repeat unit (*N*), the possible conformations (rotamers) increase non-linearly, obeying a  $4^{(N-1)}$  function due to the rotational freedom between the fluorene rings. A series of 9,9-dialkylfluorene oligomers (*N* = 1,2,3,5,7) (Chart 5) dissolved in various alkanes, alcohols and other solvents permits discussion of CPL/PL and CD/UV-visible spectral characteristics as functions of *N* and solvent viscosity based on knowledge of Sections 2.2–2.5.

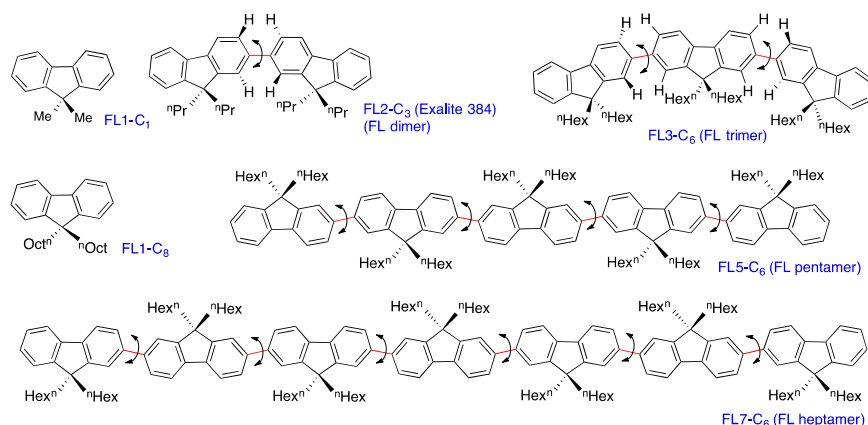


**Chart 5.** Chemical structures of 9,9-dimethylfluorene (FL1-C<sub>1</sub>), 9,9-di-*n*-octylfluorene (FL1-C<sub>8</sub>), 9,9,9',9'-tetrakis(*n*-propyl)-2,7'-difluorene (Exalite 384), 9,9,9',9',9'',9''-hexakis(*n*-hexyl)-2,7';2',7''-trifluorene (FL3-C<sub>6</sub>), 9,9,9',9',9'',9''',9''''',9''''''-decakis(*n*-hexyl)-2,7';2',7''',2''',7''''',2''''',7''''''-pentafluorene (FL5-C<sub>6</sub>), 9,9,9',9',9'',9''',9''''',9''''''',9''''''',9''''''''-dodecakis(*n*-hexyl)-2,7';2',7''',2''',7''''',2''''',7''''''',2''''''',7''''''''-heptafluorene (FL7-C<sub>6</sub>).

First of all, the CPL/PL spectra of 9,9-dimethylfluorene (FL1-C<sub>1</sub>) and 9,9-dioctylfluorene (FL1-C<sub>8</sub>) in methanol and a higher viscous *n*-undecanol (16.95 cP) are compared in Figure 7a,b. Although CD Cotton effects at the corresponding UV bands for FL1-C<sub>1</sub> and FL1-C<sub>8</sub> in methanol are not detectable (Figure S5a,b) in SM), very weak CPL signals are nevertheless apparent; a bisignate CPL band for FL1-C<sub>1</sub> in methanol can be seen, although for FL1-C<sub>1</sub> in *n*-undecanol and FL1-C<sub>8</sub> in methanol and *n*-undecanol, weak (–)-sign CPL bands are reproducibly observed (Figure 7a,b and Figure S5c,d) in SM). These FL monomers at the S<sub>1</sub> state may be slightly distorted because of two alkyl groups located at the same 9,9-positions. These  $g_{lum}$  values, on the order of 10<sup>−4</sup> and with a (–)-sign, are negligibly small when compared to those of oligofluorenes ( $N = 2–7$ ), as shown in the flowing.

Next, the CPL/PL spectra of Exalite 384 (a fluorene dimer, FL2-C<sub>3</sub>), bearing *n*-propyl groups in the 9,9'-positions, in several solvents were compared (Figure 8a–c and Figure S6a–c) in SM), including for reference the CD/UV-visible spectra in methanol (Figure S6d) in SM). The fluorene dimer clearly showed (–)-sign vibronic CPL signals at 360–380 nm. In lower viscosity solvents such as methanol, *n*-pentane and chloroform (0.55 cP), the  $g_{lum}$  values are of the order of  $-(0.05\sim 0.2) \times 10^{-3}$  (Figure 8a and Figure S6a,c) in SM). However, in *n*-hexadecane (3.47 cP), *n*-undecanol (16.95 cP) and the branched hydrocarbon, squalene (29.5 cP), the  $g_{lum}$  values increase to  $-0.5 \times 10^{-3}$ ,  $-0.9 \times 10^{-3}$  and  $-1.1 \times 10^{-3}$ , respectively (Figure 8b,c and Figure S6b) in SM). The  $g_{lum}$  value was plotted as carbon numbers of *n*-alkanes ( $N = 5–16$ ) and *n*-alkanols including methanol and ethanol ( $N = 1–11$ ) in Figure 8d. It is obvious that the  $g_{lum}$  value increases discontinuously with increase of the carbon numbers in the two series of *n*-alkanes and *n*-alkanols. Larger carbon numbers increase the viscosity due to an increase in London dispersion interactions and energy.

This tendency led us to plot the  $g_{lum}$  value as a function of solvent viscosity using thirty-two kinds of molecular liquids, including twelve alkanes (linear and branched), eighteen alcohols (linear, branched and cyclic) and chloroform (Figure 8e,f). The  $g_{lum}$  value increased but underwent a discontinuous step-like transition when  $[\eta] = 4–9$  cP and  $11–30$  cP (Figure 8e). The  $g_{lum}$  value increased almost linearly in response to solvent viscosity when  $[\eta]$  was in the range 0.21 (*n*-pentane) to  $[\eta] = 4.59$  (*n*-hexanol) (Figure 8e,f).



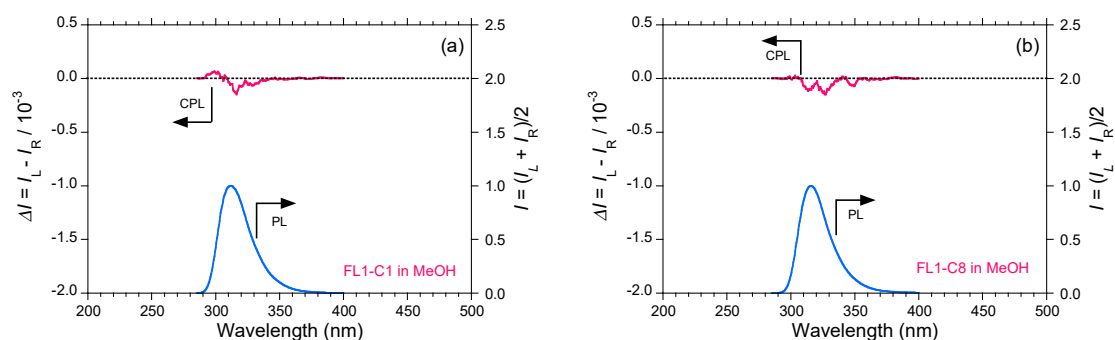


**Figure 7.** CPL/PL spectra of (a) FL1-C<sub>1</sub> excited at 255 nm and (b) FL1-C<sub>8</sub> excited at 255 nm at room temperature in methanol. Path length: 10 mm, cylindrical cuvette, conc.:  $5 \times 10^{-5}$  M.

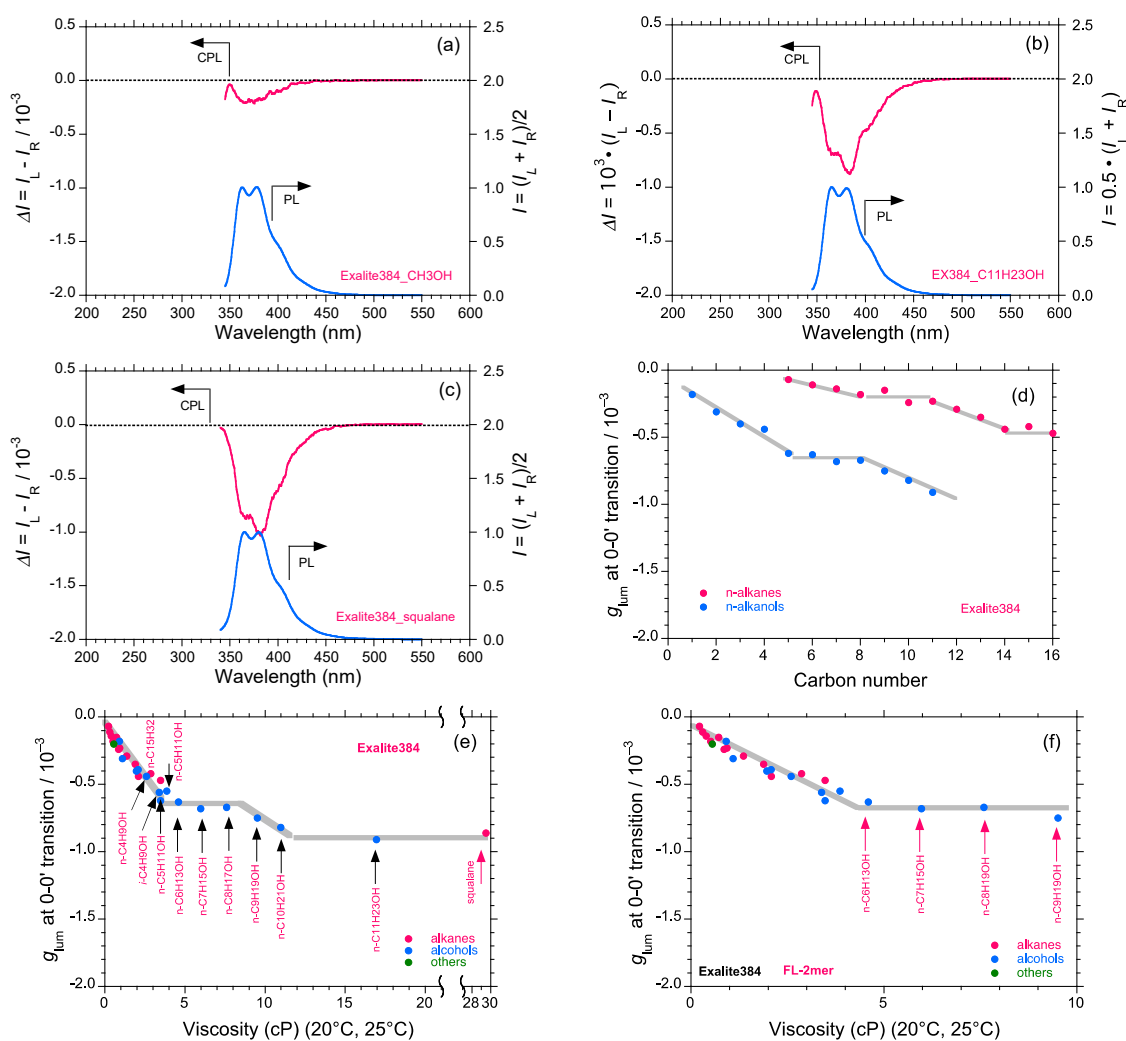


**Figure 8.** CPL/PL spectra of FL2-C<sub>3</sub> (Exalite 384, fluorene dimer) excited at 315 nm at room temperature (a) in methanol, (b) in *n*-undecanol and (c) in squalene; (d) the  $g_{lum}$  value at 0-0' band of FL2-C<sub>3</sub> as a function of carbon numbers in two series of *n*-alkanes and *n*-alkanols including methanol and ethanol; (e) the  $g_{lum}$  value at the 0-0' band of FL2-C<sub>3</sub> (Exalite 384) as a function of viscosity (in cP at 20–25 °C) in various achiral alkanes, alkanols and other solvents and (f) magnification of the viscosity region 0–10 cP. Path length: 10 mm, cylindrical cuvette, conc.:  $1 \times 10^{-5}$  M.

The quantized, two-step-like phase transition behaviors should be closely related to structural reorganization at the  $S_1$  state. A possible explanation for the quantized  $g_{lum}-[\eta]$  relation arises from anti-syn structural reorganization occurring at the  $S_1$  state associated with a change in preference in twisted geometry between left and right. Exalite 384 in solution at the  $S_0$  state should exist as a mixture of two enantiomeric pairs of anti and syn forms, as proven by the lack of CD signals at 320 nm for the  $\pi-\pi^*$  transition of the fluorene rings. The less polar anti-form is energetically more stable than the polar syn form. However, Exalite 384 at the  $S_1$  state prefers the polar syn-form with a handed twist due to suppression of ro-vibrational modes along the single C–C bond between the two fluorene rings when  $[\eta]$  is sufficient high. At the first transition when  $[\eta] = 5-7$  cP, Exalite 384 adopts the anti-form with a *P*-screw sense (dihedral angle between fluorene ring  $+40^\circ$ ) exhibiting (–)-sign CPL signals. At the second transition when  $[\eta] > 11$  cP, Exalite 384 adopts the more stable syn form with an *M*-screw sense (dihedral angle between fluorene ring  $-40^\circ$ ), exhibiting (–)-sign CPL signals.

The  $g_{lum}-[\eta]$  relation of the fluorene dimer bearing *n*-propyl side chains (Exalite 384) prompted us to further investigate the fluorene-ring number (*N*) dependence of the CPL/PL and CD/UV-visible spectral characteristics in three fluorene oligomers bearing *n*-hexyl groups, including a fluorene trimer (FL3-C<sub>6</sub>), a fluorene pentamer (FL5-C<sub>6</sub>) and a fluorene heptamer (FL7-C<sub>6</sub>).

The CPL/PL spectra of FL3-C<sub>6</sub> are displayed in Figure 9a–e and Figure S7a–c in SM and for comparison CD/UV-visible spectra in ethanol are given in Figure S7d in SM. FL3-C<sub>6</sub> reveals clear CPL signals at the same wavelength as the PL in the emission spectra in low viscosity solvents like *n*-pentane (0.21 cP, Figure 9a), diethylether (0.22 cP, Figure 9b), dichloromethane (0.41 cP, Figure 9c), ethanol (1.09 cP, Figure 9d), acetone (0.31 cP, Figure S7a in SM), tetrahydrofuran (0.46 cP, Figure S7b in SM) and can also be observed in higher viscosity solvents including *n*-undecanol (16.95 cP, Figure 9e) and squalene (29.5 cP, Figure S9c in SM). By testing with twelve *n*-alkanes, fourteen alkanols (linear and branched) and seven other types of solvents (diethylether, THF, chloroform, dichloromethane, acetone, isooctane and squalene), the full-range  $g_{lum}-[\eta]$  and its zoomed-in  $g_{lum}-[\eta]$  relations were evaluated and are plotted in Figure 9g,h, respectively. The  $g_{lum}$  value as a function of carbon numbers of *n*-alkanes and *n*-alkanols including ethanol indicated step-like transitions at specific carbon numbers, indicating that the effect is a function of  $[\eta]$  value and does not depend on the chemical identity of the alkane or alkanol (Figure 9f). The  $g_{lum}$  values tended to alter linearly in two steps when  $[\eta]$  is in the ranges between 0.2 to 1.0 cP and from 1 to 6 cP. Eventually, the  $g_{lum}$  value leveled off at  $-1.40 \times 10^{-3}$  at 390 nm when  $[\eta] > 7$  cP.

Similar tendencies in the CPL/PL/CD/UV-visible spectral characteristics of FL5-C<sub>6</sub> can be seen in several solvents of lower and higher viscosity (Figure 10a–d and Figure S8a–b) in SM). FL5-C<sub>6</sub> revealed significant CPL signals at the corresponding PL emissions, regardless of solvent viscosity. By using twelve *n*-alkanes, fourteen alkanols (linear and branched) and six other types of solvents (diethylether, THF, chloroform, dichloromethane, acetone and squalene), the full-range  $g_{lum}-[\eta]$  and its zoomed-in  $g_{lum}-[\eta]$  relations were evaluated and are plotted in Figure 10e,f, respectively. The  $g_{lum}$  value as a function of carbon numbers of *n*-alkanols including ethanol indicated a clear transition at a carbon number of four (Figure S8d in SM). From Figure 10e–f, the  $g_{lum}$  values tended to alter linearly in two steps when the  $[\eta]$  value was in the ranges 0.2 cP to 0.7 cP and 0.7 cP to 4 cP. Eventually, the  $g_{lum}$  value leveled off at  $-1.44 \times 10^{-3}$  at 407 nm when  $[\eta] > 4$  cP.

Very similar CPL/PL/CD/UV-visible spectral characteristics for FL7-C<sub>6</sub> were also confirmed (Figure 11a–d and Figure S9a–d in SM). For comparison, CD/UV-visible spectra in ethanol are given in Figure S9e in SM. FL7-C<sub>6</sub> revealed clear CPL signals at the corresponding to PL spectra in low viscosity solvents (*n*-pentane, diethylether, dichloromethane, acetone and chloroform) and in viscous solvents like *n*-undecanol and *n*-hexadecane. By using the same series of *n*-alkanes and alkanols and other types of solvents used for FL5-C<sub>6</sub>, the full-range  $g_{lum}-[\eta]$  and its zoomed-in  $g_{lum}-[\eta]$  relations were evaluated and are plotted in Figure 11e,f, respectively. The  $g_{lum}$  value as a function of carbon numbers of *n*-alkanes and *n*-alkanols including ethanol indicated transitions when the carbon numbers in the *n*-alkanes was four and in *n*-alkanols was six and nine (Figure S9f in SM). The  $g_{lum}$  values alter linearly

in one-step only when  $[\eta]$  is in the range from 0.2 cP to 0.6 cP. Eventually, the  $g_{lum}$  value leveled off at  $-1.25 \times 10^{-3}$  at 412 nm when  $[\eta] > 0.6$  cP.

Four other commercially available fluorene analogs, Exalite 376 (dibenzofuran dimer), Exalite 404 (*p*-phenylene connected to two fluorenes), Exalite 428 (fluorene trimer bearing two *p*-*tert*-butylphenyl groups) and Exalite 416 (fluorene dimer bearing two *p*-anisyl groups) (Chart 6), showed similar  $g_{lum}$ - $[\eta]$  tendencies over a broad range of  $[\eta]$  values (Figure 12a–f). Exalite 376 and Exalite 384 are in the same category because they have one rotatable C–C single bond between the two fluorenes or two dibenzofurans. Similarly, Exalite 404, Exalite 384, Exalite 416 and FL3-C<sub>6</sub> are in the same category because they have two rotatable C–C single bonds between three fluorenes (and *p*-phenylene), if the very floppy end-termini of the two aryl groups are ignored. With further increase in the fluorene ring number from three to five and seven, the absolute  $g_{lum}$  value tended to decrease slightly.

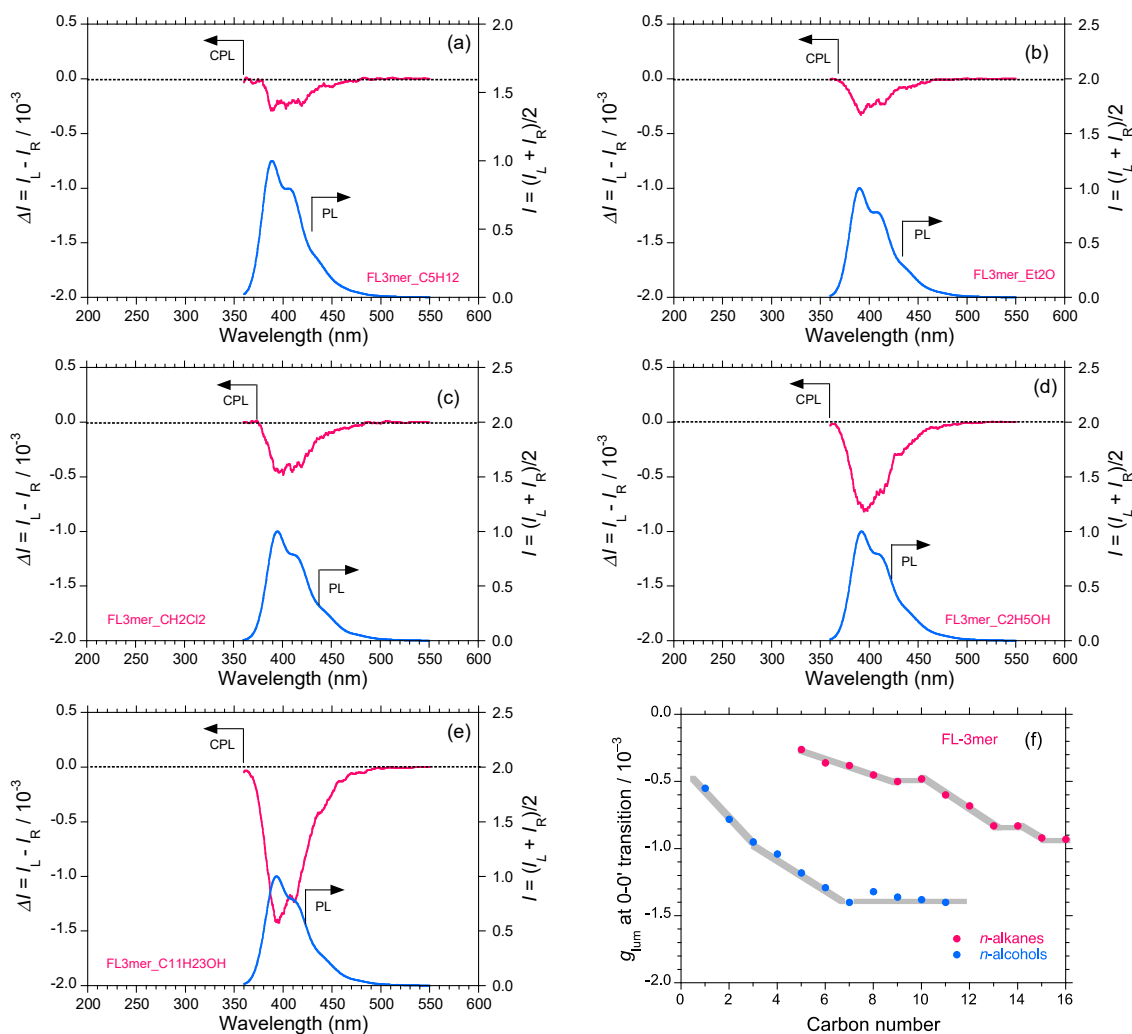


**Figure 9.** CPL/PL spectra of FL3-C<sub>6</sub> (fluorene trimer) excited at 330 nm at room temperature (a) in *n*-pentane, (b) in diethylether, (c) in dichloromethane, (d) in ethanol and (e) in *n*-undecanol; (f) The  $g_{lum}$  value at 0-0' band of FL3-C<sub>6</sub> as a function of carbon numbers in two series of *n*-alkanes and *n*-alkanols (including ethanol); (g) the  $g_{lum}$  value at the 0-0' band of FL3-C<sub>6</sub> as a function of viscosity (in cP at 20–25 °C) of various achiral alkanes, alkanols and other solvents and (h) magnification of the viscosity region 0–2.0 cP. Path length: 10 mm, cylindrical cuvette, conc.:  $2 \times 10^{-5}$  M.

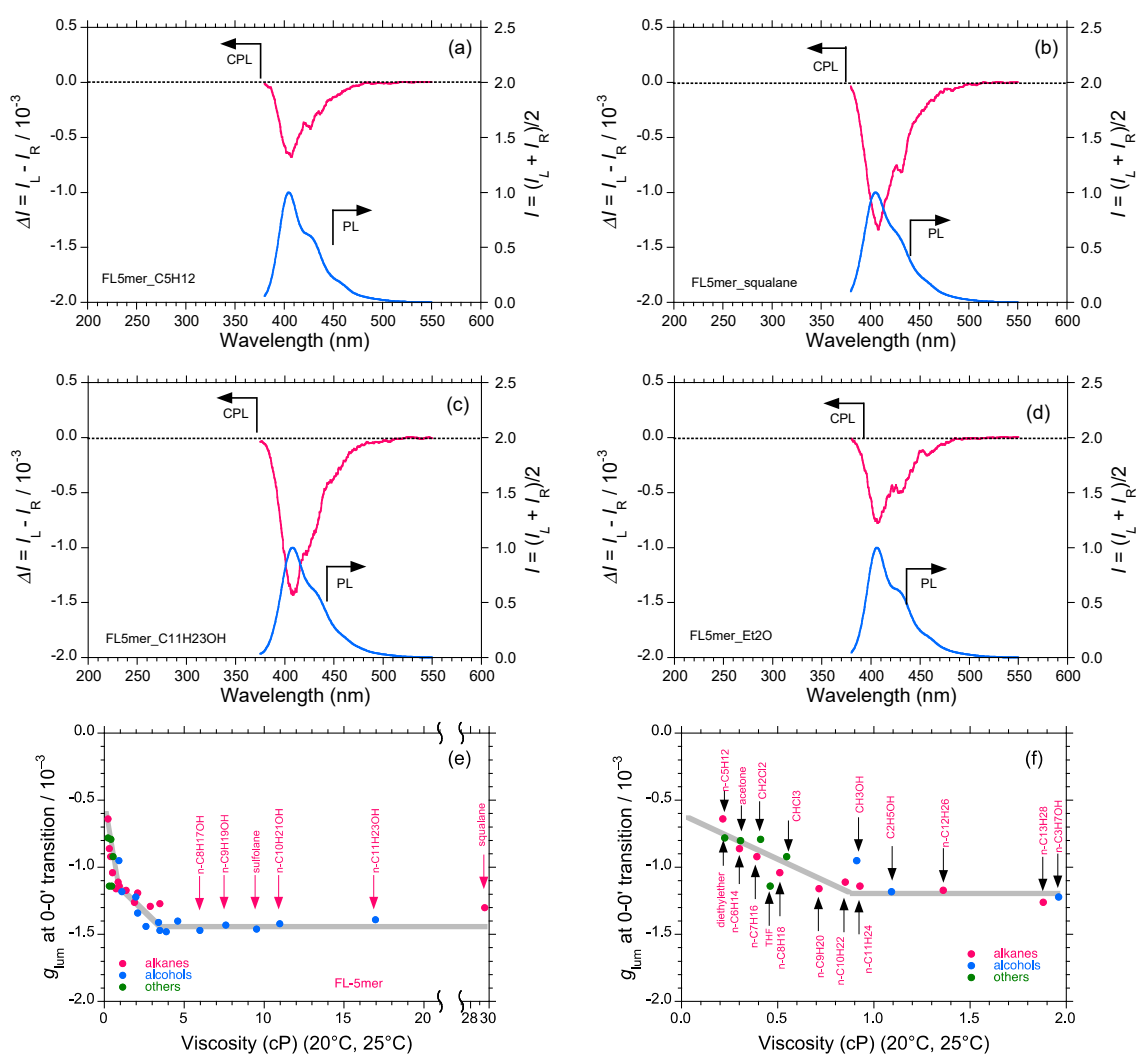


**Figure 10.** CPL/PL spectra of FL5-C<sub>6</sub> (fluorene pentamer) excited at 340 nm at room temperature (a) in *n*-pentane, (b) in squalane, (c) in *n*-undecanol and (d) in diethylether; (e) the  $g_{lum}$  value at the 0-0' band of FL5-C<sub>6</sub> as a function of viscosity (in cP at 20–25 °C) of various achiral alkanes, alkanols and other solvents and (f) magnification of the viscosity region 0–2.0 cP. Path length: 10 mm, cylindrical cuvette, conc.:  $5 \times 10^{-6}$  M.

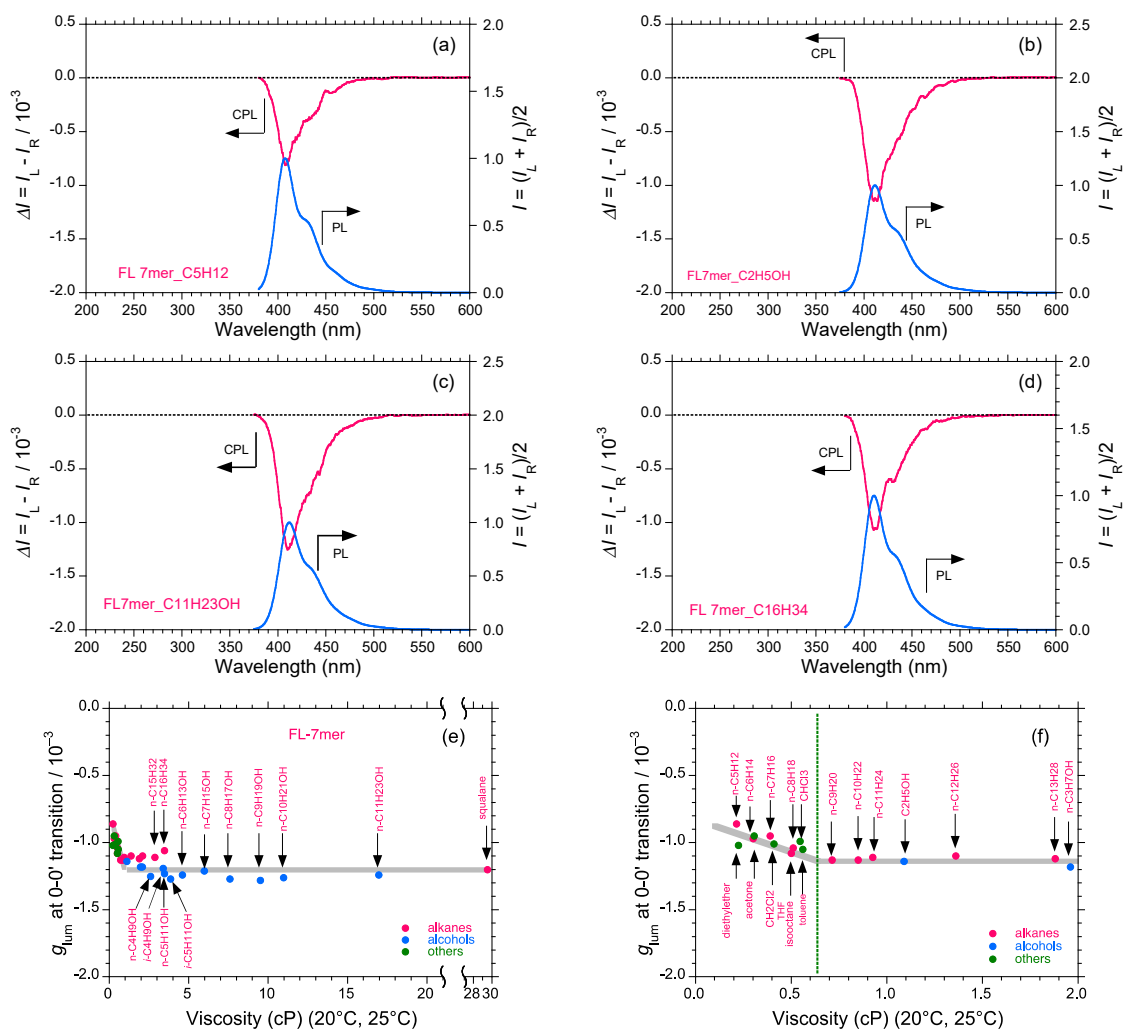


**Figure 11.** CPL/PL spectra of FL7- $C_6$  (fluorene heptamer) excited at 350 nm at room temperature (a) in *n*-pentane, (b) in ethanol, (c) *n*-undecanol and (d) in *n*-hexadecane; (e) the  $g_{lum}$  value at the 0-0' band of FL7- $C_6$  as a function of viscosity (in cP at 20–25 °C) of various achiral alkanes, alkanols and other solvents and (f) magnification of the viscosity region 0–2.0 cP. Path length: 10 mm, cylindrical cuvette, conc.:  $5 \times 10^{-6}$  M.

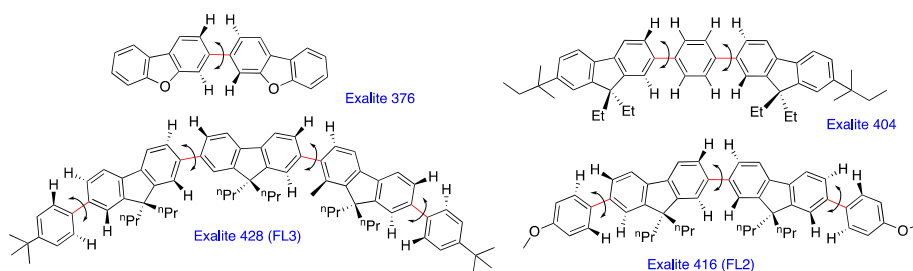


**Chart 6.** Chemical structures of 3,3'-bidibenzo[b,d]furan (Exalite 376), 1,4-bis(9,9-diethyl-7-(*t*-pentyl)-9H-fluoren-2-yl)benzene (Exalite 404), 7,7''-bis(4-(*t*-butyl)phenyl)-1-methyl-9,9,9',9',9''-hexapropyl-9H,9'H,9''H-2,2':7':2''-terfluorene (Exalite 428) and 7,7'-bis(4-methoxyphenyl)-9,9,9',9'-tetrapropyl-9H,9'H-2,2'-bifluorene (Exalite 416).

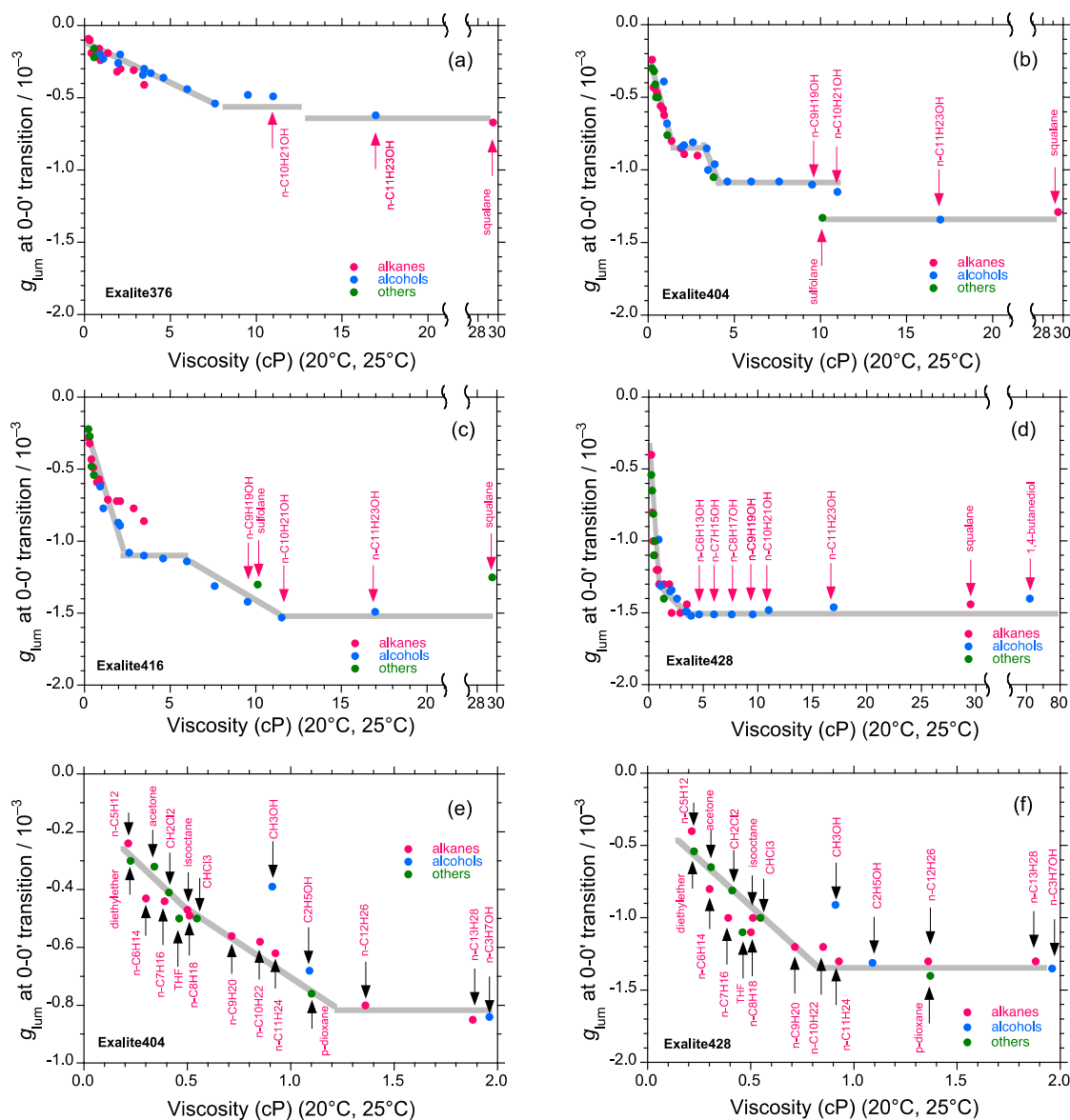


**Figure 12.** The  $g_{lum}$  value at the 0-0' band of (a) Exalite 376, (b) Exalite 404, (c) Exalite 416 and (d) Exalite 428 as a function of the viscosity (in cP at 20–25 °C) of various achiral alkanes, alcohols and other solvents (0–30 cP). The magnified plots of  $g_{lum}$  value at 0-0' band of (e) Exalite 404 and (f) Exalite 428 as a function of the viscosity (in cP at 20–25 °C) of various achiral alkanes, alcohols and other solvents (0–2.0 cP). Path length: 10 mm, cylindrical cuvette, conc.:  $1 \times 10^{-5}$  M.

To this end in the study of the chiroptical characteristics in the fluorene family at the  $S_1$  state, we compared the CPL and PL spectra of FL1-C<sub>8</sub>, Exalite 384, Exalite 404, Exalite 428, FL3-C<sub>6</sub>, FL3-C<sub>6</sub>, FL5-C<sub>6</sub> and FL7-C<sub>6</sub> dissolved in *n*-undecanol (16.95 cP) in Figure 13a. The  $\lambda_{ext}$  peak wavelength of the vibronic luminescence bands at the 0-0' transition progressively redshifted as the fluorene ring number increased from one to seven. The magnitude of the CPL signal,  $\Delta I = I_L - I_R$ , increased when the ring number was greater than three (regarding Exalite 404 as a fluorene trimer).

From the empirical  $g_{lum}$ - $[\eta]$  relations of Exalite 384, FL3-C<sub>6</sub>, FL5-C<sub>6</sub>, FL7-C<sub>6</sub>, Exalite 376, Exalite 404, Exalite 428 and Exalite 416 (Figure 8e–h, Figure 10e,f, Figure 11e,f and Figure 12a–f), it becomes apparent that the  $[\eta]$  value may be extrapolated to a non-zero  $g_{lum}$  value with (–) sign when  $[\eta]$  is 0.0 cP, corresponding to solvent-free, collision-free conditions. This tendency is remarkable in the cases of FL5-C<sub>6</sub> (Figure 10f) and FL7-C<sub>6</sub> (Figure 11f). For  $g_{lum}$  values at  $[\eta] > 30$  cP, this tendency

is obvious as a function of fluorene ring number (Figure 13b). It is clear that the absolute  $g_{lum}$  value increases when  $N = 1-3$  and levels off at  $N = 5$  and decreasing slightly when  $N = 7$ .

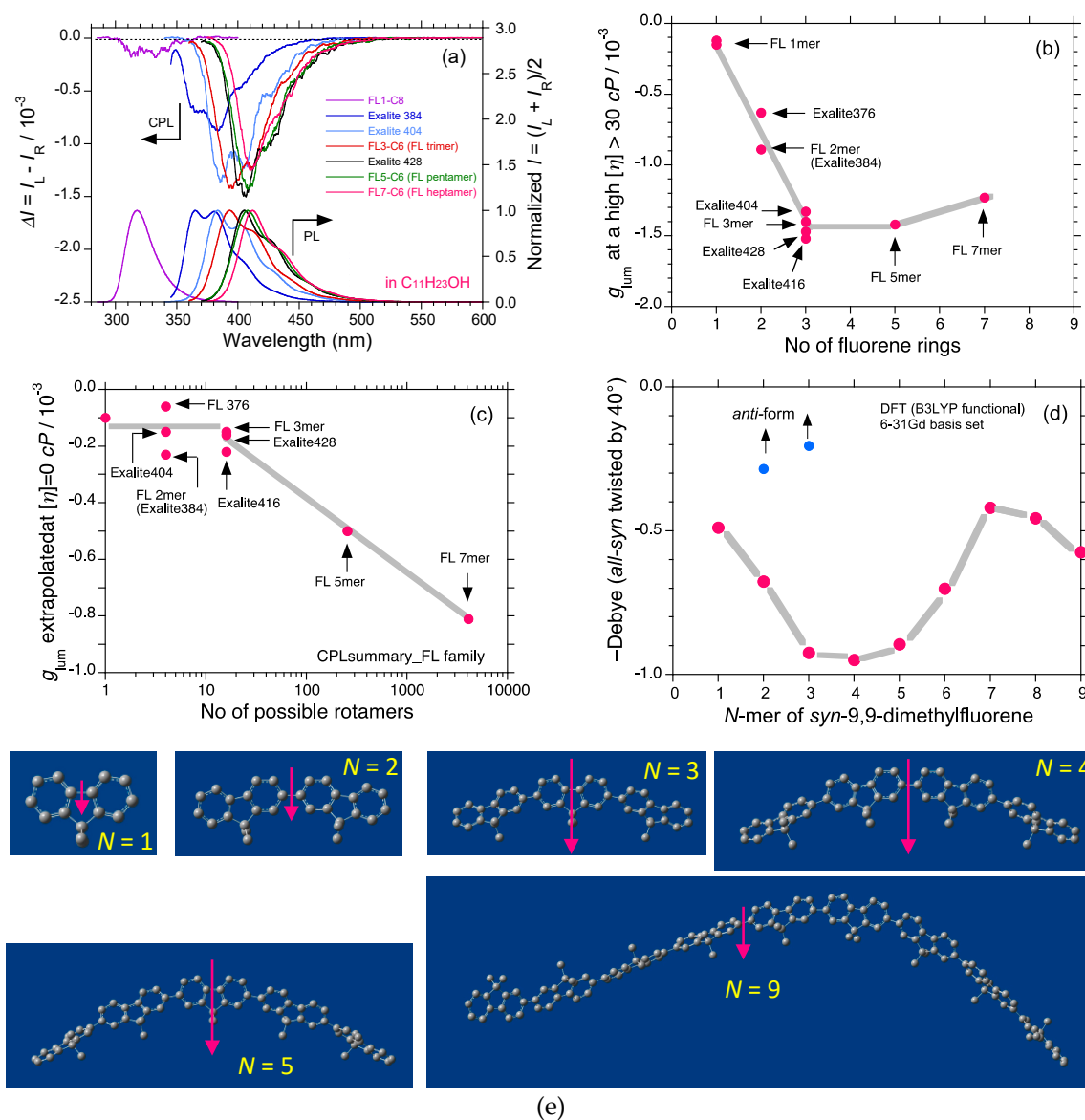


**Figure 13.** (a) Comparisons of CPL and PL spectra at the 0-0' band of FL1-C<sub>8</sub>, Exalite 384, Exalite 404, FL3-C<sub>6</sub>, Exalite 428, FL5-C<sub>6</sub> and FL7-C<sub>6</sub> in  $n$ -undecanol; (b) the  $g_{lum}$  value at the 0-0' band extrapolated at  $[\eta] > 30$  cP of FL1-C<sub>8</sub>, Exalite 384, Exalite 404, FL3-C<sub>6</sub>, Exalite 428, FL5-C<sub>6</sub> and FL7-C<sub>6</sub> as a function of the fluorene ring number; (c) the  $g_{lum}$  value at the 0-0' band extrapolated at  $[\eta] = 0.0$  cP of FL1-C<sub>8</sub>, Exalite 384, Exalite 404, FL3-C<sub>6</sub>, Exalite 428, FL5-C<sub>6</sub> and FL7-C<sub>6</sub> as a function of possible rotational isomers of these fluorenes; (d) the dipole moments (in Debye) of hypothetical 9,9-dimethylfluorene  $N$ -mers, adopting a syn-geometry twisted by 40° in a vacuum as a function of repeat number  $N$ . For comparison, the dipole moments (in Debye) of hypothetical 9,9-dimethylfluorene dimer and trimer, adopting an anti-geometry twisted by 40° in a vacuum were marked in blue dots. These dipole moments were obtained using DFT (B3LYP with 6-31G(d) basis set); (e) optimized models of fluorene  $N$ -mer ( $N = 1-5$  and 9), the molecular models of the 9,9-dimethylfluorene  $N$ -mer with  $N = 1, 2, 3, 4, 5$  and 9, optimized by DFT. The red arrow stands for the relative magnitude of the dipole moments. As  $N$  increases from 1 to 5, the dipole moment increases monotonically, while when  $N = 9$ , the dipole moment abruptly decreases due to a partial cancellation of the moments in the case of a helical geometry that is uniformly twisted by 40° macroscopically.

To explain this tendency, we assumed that photoexcited fluorene  $N$ -mers in the  $S_1$  state prefer a polar geometry, adopting the syn-form with  $+40^\circ$  twists. Molecular models of the 9,9-dimethylfluorene  $N$ -mers ( $N = 1, 2, 3, 4, 5$  and  $9$ ) optimized by DFT calculation (B3LYP functional with 6-31G(d) basis set) are illustrated in Figure 13e. The red arrow relates to the relative magnitude of the dipole moments. As the  $N$ -number increases from 1 to 3, the dipole moment increases monotonically. However, the magnitude of the dipole moments leveled off at  $N = 3-5$  and then decreased for  $N = 5-7$  due to the mutual cancellation between all the moments of the macroscopically twisted helical geometry (Figure 13e,  $N = 9$ ). For comparison, the fluorene  $N$ -mers ( $N = 2, 3$ ) with anti-form twisted by  $+40^\circ$  are less polar and more likely to depend weakly on  $N$  (blue filled circles, Figure 13e). Possibly fluorene  $N$ -mers ( $N \geq 2$ ) in the  $S_1$  state may adopt a similar twisted syn-form rather than a twisted anti-form.

The numbers of rotamers in these compounds, arising due to the degree of freedom, is connected to cosmological entropy in the Big Bang Universe [84–86]. A larger number of rotamers means a high entropy state and conversely, one rotamer indicates zero entropy. The rotational barrier ( $E_b$ ) in oligo- and polyfluorenes is as small as  $\sim 0.6$  kcal mol $^{-1}$  per C–C single bond between the rings [87]. This small  $E_b$  value allows for generation of all possible rotamers in a statistical fashion under thermodynamic equilibrium since the thermal energy at 300 K is  $\sim 0.6$  kcal mol $^{-1}$ . Although Exalite 384 with one rotatable C–C bond has four possible rotamers (syn- and anti-) with  $P$ - and  $M$ -twists as mentioned above, FL7-C $_6$  can in principle adopt 4096 rotamers as it has six rotatable C–C bonds. Thus, FL7-C $_6$  in the highest entropy  $S_0$  state reveals the greatest (–)-sign  $g_{lum}$  value arising from temporal generation of a few rotamers on the order of  $\sim 10^{-8}$  s obeying Kasha's rule.

We re-plotted the  $g_{lum}$  value extrapolated at  $[\eta] = 0$  cP as a function of the number of possible rotamers in a family of nine fluorenes on a logarithmic scale (Figure 13c). Although the  $g_{lum}$  value at zero-viscosity shows a constant value of  $\sim -0.2 \times 10^{-3}$ , up to possible rotamers ( $\sim 15$ ), the value increases exponentially and levels off at  $\sim -0.8 \times 10^{-3}$  as the number of possible rotamers increases. The  $g_{lum}$  value at zero-viscosity implies that the photoexcited oligofluorenes will emit CPL signals with (–)-sign even under collision-free conditions, such as, for example, in a vacuum.

### 3. Discussion

One can imagine that the huge numbers of the far off fixed stars in the accelerating expanded Universe, excepting our solar sun, are faintly shining as a result of proton-proton chain reactions between hydrogen atoms that are producing deuterium, positrons and neutrinos, induced by the  $PV$  weak nuclear force mediated by the charged  $W^+$  boson [88]. Due to a high Coulombic barrier height between repulsive protons, the reactions occur only very slowly by a tunneling mechanism [88]. Due to the intensity of the light from our sun, and its subsequent scattering in the earth's atmosphere by dust, water mist and other materials, the faintly shining stars are not apparent at all during the daytime. However, people can enjoy the shining only at nighttime when the influence of the sun is absent.

Similarly, if one wishes to detect the weak shining chiroptical signals coming from the inherent left-right imbalance between enantiomers due to the  $PV$ -weak nuclear force originating from the neutral  $Z^0$  boson, it is necessary to remove completely any influences of the parity-conserving  $EM$  force between enantiomers, that already adopt chirally distorted rigid frameworks due to the existence of point chirality and/or atropo chirality. A CPL spectropolarimeter which measures steady state systems may be regarded as a 'desk-top low-energy spinning photon–molecule collider decelerator' as it allows for the detection of the subtle difference in left- and right-handed light speed between enantiomers at the  $S_1$  state, which are temporally generated with lifetimes on the order of several  $10^{-9}$  s during irradiation of an unpolarised photon source, while a CD spectropolarimeter, operating on the timescale of  $10^{-15}$  s and based on the Franck-Condon principle is the low-energy photon–molecule interaction analyzer to detect differences between thermally stable enantiomers with long lifetimes at the  $S_0$  state.

The CPL spectrometer can excite huge numbers of molecular luminophores at once. In the relaxation process from the  $S_1$  to  $S_0$  state in a cylindrical cuvette (path length 1.0 cm,  $10^{-6}$ – $10^{-5}$  M) with front-side lens-focused beam ( $\sim 1$  mm in diameter), approximately,  $10^{13}$ – $10^{14}$  molecules are excited



simultaneously and macroscopically. The relaxation process obeys the *arrow of time* proposed by British astronomer, Arthur Eddington in 1927 [89]; this concept means that entropy increases spontaneously as time goes by. The arrow of time implies the asymmetry of time that discriminates between future, present, and past. This direction is pre-determined by organization of subatoms, atoms, molecules, polymers and life in the framework of the four-dimensional relativistic world. If it is possible to extend the concept to the issue of spontaneous and/or mirror symmetry- breaking (MSB) and MPV hypotheses, the left-right direction is pre-determined by the PV-WNC, which is mediated by a handed  $Z_0$  boson and for non-rigid photoexcited molecules result in a preference to radiate right-handed circularly polarized light.

When the molecules are excited by photon sources, the PMT detector of the CPL spectrometer (present) can detect the passage of radiation (past) at the  $S_1$  state, an event which occurred  $10^{-9}$  s before, whilst the PMT detector of the CD spectrometer (present) can see the passage of absorption at the  $S_0$  state which occurred  $10^{-15}$  s before (past) based on the Franck–Condon principle and the Kasha’s rule in the Jablonski diagram [66,67,90].

In the past, our Universe experienced in the past three major phase transitions as a consequence of three broken symmetries to produce four fundamental physical forces that govern our life and matter worlds [91–94]. The timeline from the Big Bang (BB) to present is considered as follows:

The four forces were unified in the beginning of the Universe, at the so-called Planck time ( $\sim 10^{-44}$  s after BB). Then firstly, the unified force bifurcated into gravitational and strong-and-electroweak forces at  $\sim 10^{-42}$  s, followed by bifurcation of the strong-and-electroweak force into strong and electroweak forces at  $\sim 10^{-34}$  s. Eventually, at  $\sim 10^{-12}$  s, the electroweak force bifurcated into the electromagnetic and weak forces, producing unequal bosons (massive  $W^\pm$  and  $Z^0$  and the massless photon). This event occurred in a period of *ca.*  $10^{-15}$  s, and as an event shorter than  $10^{-12}$  s governed by the electroweak force, may maintain mirror symmetry. However, for events occurring over a period of  $10^{-9}$  s, i.e., longer than  $10^{-12}$  s, it is possible to break the mirror symmetry governed by the weak force. Thus, an event timescale of  $\sim 10^{-12}$  s may be critical in the question of whether one can detect mirror symmetry conservation or mirror symmetry breaking spectroscopically.

As mentioned in the Introduction, Hund showed a theoretical relationship between molecular chirality and optical activity for a hypothetical chiral molecule in a mirror symmetric DW [1,2]. Based on the idea of time-dependent, non-stationary states of a hypothetical chiral molecule in the DW and quantum tunneling, the theory showed a solution in which the tunneling causes energy splitting,  $\Delta E_\pm$ , in the DW, leading to a spontaneous oscillation in chirality and optical activity with a dynamic racemization time ( $T_{\text{rac}}$ ) [1–3,34].

$$\Delta E_\pm = 1/2 \cdot \pi^{-1/2} \cdot (h\nu E_b)^{1/2} \cdot \exp(-E_b/h\nu) \quad (1)$$

where  $E_b$  is the height of the energy barrier at the  $S_0$  state and is possibly also applicable to the  $S_1$  state,  $\nu$  is the frequency for the vibration in a single-well,  $h$  is Planck’s constant.

Also, the relationship between energy splitting and racemization time [1,2] may be given as

$$T_{\text{rac}} = h/\Delta E_\pm \quad (2)$$

From Equation (1), the tunneling-dependent racemization time is predominantly determined by the value of  $E_b$ , and has no temperature ( $T$ ) dependency. This situation is very different from that of the thermally activated racemization process expressed by the Arrhenius equation,  $k = A \cdot \exp(-E_B/(N \cdot k_B \cdot T))$ , where  $k$  is the rate constant,  $k_B$  is the Boltzmann constant,  $N$  is Avogadro’s number, and  $A$  is the collision factor. A demarcation between the tunneling and Arrhenius-type racemizations will be that the tunneling occurs when  $E_b/Nk_B T < 10$  ( $\sim 6$  kcal mol $^{-1}$ ) and the thermally racemization is a dominant process when  $E_b/Nk_B T > 30$  ( $\sim 20$  kcal mol $^{-1}$ ). Actually, the  $E_b$  value for the inversion of ammonia is 5.8 kcal mol $^{-1}$  [1,4]. Stochastic behavior is expected, when  $10 < E_b/Nk_B T < 30$ . The idea of the  $E_b/Nk_B T$  relation might be applicable to the metastable  $S_1$  state.

To view schematically the  $E_b$ - $T_{\text{rac}}$  relationship,  $T_{\text{rac}}$  is illustrated (in s) as a function of  $E_b$  (in  $\text{kcal mol}^{-1}$ ) in *log-log* plots as shown in Figure 14. For simplicity, we chose one adjustable parameter,  $c_0 = 0.10 \dots 10.0$  with intervals of 0.10; the constant is  $10^{-10} \cdot \sqrt{\pi}$  and  $h\nu$  is fixed at 0.110. The value of  $T_{\text{rac}}$ , that is the lifetime of one enantiomeric species, is  $10^{-8}$  s, the representative lifetime of fluorescence, when  $E_b$  is  $0.7 \text{ kcal mol}^{-1}$ . The  $T_{\text{rac}}$  value becomes  $10^{-3}$  s longer, the representative lifetime of phosphorescence, when  $E_b$  slightly increases to  $2.0 \text{ kcal mol}^{-1}$ . Moreover, the  $T_{\text{rac}}$  value becomes 115 days, the representative long lifetime of stable chirality, when  $E_b$  increases to  $5.0 \text{ kcal mol}^{-1}$ . Under these conditions, stable optical activity at the  $S_0$  and  $S_1$  states is observable as CD and CPL signals. The next requirement is how the condition of  $E_{\text{pv}} \sim E_{\pm}$  is realized.

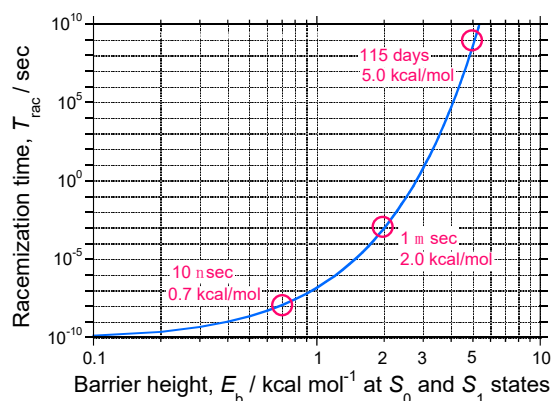


**Figure 14.** Plots of  $E_b$ -dependent  $T_{\text{rac}}$  relationship, while  $T_{\text{rac}} = 10^{-10} \cdot \sqrt{\pi} / \sqrt{c_0 \cdot 111} \exp(c_0 / 0.110)$ ;  $c_0 = 0.1$ – $10.0$  with 0.10 interval.

The  $E_b$ - $T_{\text{rac}}$  relationship, as demonstrated in previous sections, can be categorized in three cases: (1) no detectable CD or CPL signals at the  $S_1$  and  $S_0$  states due to inherent molecular achirality, exemplified by unsubstituted acenes and pyrene (Scheme 1); (2) thermally and photophysically stable CD and CPL signals at the  $S_1$  and  $S_0$  states due to rigid chiral structures with a high  $E_b$  value exemplified by *D*-/*L*-camphor and  $C_2$ -symmetric *R*-13/*S*-13 (Scheme 3); (3) no detectable and/or very weak CD signals at the  $S_0$  state, but noticeable CPL signals at the  $S_1$  state due to non-rigid enantiomers with a low  $E_b$  value which have rotational and flip-flop motional freedoms, as exemplified by structures in Schemes 2, 4–8, and  $C_2$ -symmetric, but rotatable *R*-14/*S*-14 and *R*-15/*S*-15 in Scheme 3. The potential energy surfaces at the  $S_1$  and  $S_0$  states are illustrated as follows:

- Case 1. Molecules in a single-well; no CD and no CPL signals are observable due to inherently achiral geometry at the  $S_0/S_1$  states (Figure 15a).
- Case 2. Rigid chiral molecules enforced by a stereocenter in a DW with sufficiently high  $E_b$  at the  $S_0/S_1$  states; for these, if a single (*S*)-enantiomer were obtained, the CD and CPL signals would be mirror-images of the (*R*)-enantiomer due to the inherent chiral geometry of the  $S_0/S_1$  states (Figure 15b). The value of  $g_{\text{lum}}$  is similar to that of  $g_{\text{abs}}$  and no change in sign between CPL and CD is expected. The stereocenter is responsible for the parity-conserving electromagnetic force.
- Case 3. Non-rigid chiral molecules in a DW with sufficiently small  $E_b$  at the  $S_0/S_1$  states; because the (*S*)-enantiomer is difficult to isolate due to rapid racemization by quantum tunneling, it is easy to be convinced that no CD or CPL signals at the  $S_0/S_1$  states can be detected, and this is the conventional wisdom among chemists and described in textbooks on stereochemistry (Figures 14d and 15c). The non-rigid chiral molecules are thus called CD-silent/CPL-silent molecules. The silence arises from quantum tunneling at the  $S_0/S_1$  states. However, if the tunneling at the  $S_1$  state is a one-way event due to the *PV*-*WNC*, one can observe (–)-CPL (*right-handed* CPL only) (Figure 15e,f). In this case, the rapid left-right oscillation at the  $S_1$  state by quantum tunneling results in no detectable CD signals.

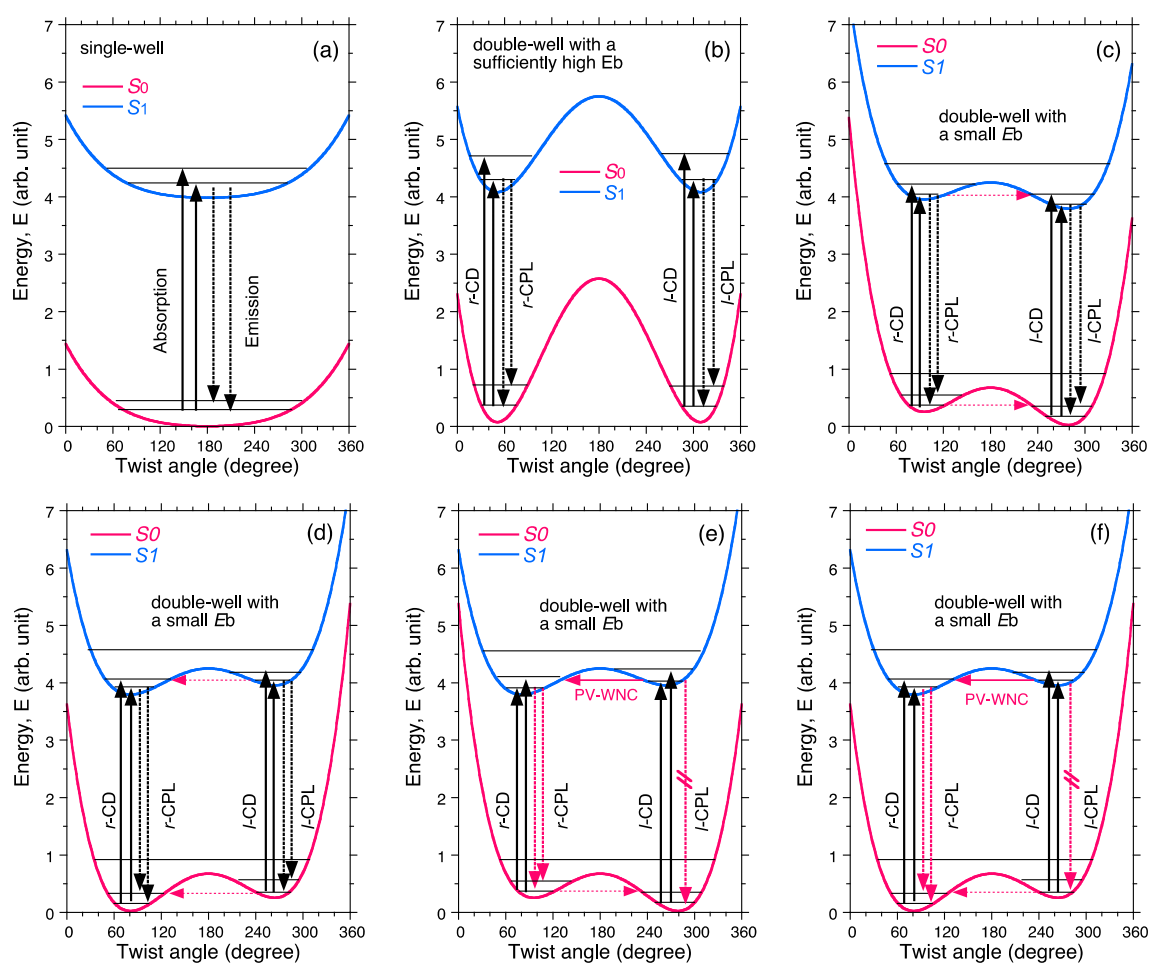


**Figure 15.** Potential energy surfaces of (a) an inherently achiral molecule in single-wells at the  $S_1$  and  $S_0$  states, (b) a rigid chiral molecule in mirror symmetric double-wells with a sufficiently large  $E_b$  value without tunneling at the  $S_1$  and  $S_0$  states, (c,d) a non-rigid chiral molecule in nearly mirror symmetric double-wells with small  $E_b$  values and resonance tunneling, causing parity-conserved mirror symmetric oscillations at the  $S_1$  and  $S_0$  states, and (e,f) a non-rigid chiral molecule in a nearly mirror symmetrical double-well at the  $S_1$  state with a small  $E_b$  and resonance tunneling in the presence of a handed weak neutral current, causing parity-violated non-mirror symmetric oscillation, while in a nearly mirror symmetrical double-well at the  $S_0$  state with a small  $E_b$  and resonance tunneling in the absence of the weak neutral current, causing parity-conserved mirror symmetric oscillation. Red dotted arrow means parity-conserved resonance tunneling, while red solid denotes a handed parity-violating weak neutral current origin resonance tunneling.

Open questions remain as to why the solvent viscosity discontinuously affects the (–)CPL magnitude and the major role of the solvent viscosity. To control the resonance tunneling characteristics, the  $E_b$  value is a continuous variable, but can modify the resonance characteristics because of its exponential characteristics (Equation (1)). A higher viscosity increases the  $E_b$  value, resulting thereby in a smaller  $\Delta E_{\pm}$  value. Conversely, a lower viscosity decreases the  $E_b$  value, affording a larger  $\Delta E_{\pm}$  value. The former results in slower  $T_{rac}$  and the latter in faster  $T_{rac}$ . To understand whether resonance tunneling between two sub-levels occurs, the discontinuous transition as a function of continuous external variables, like temperature, electric field, magnetic field and possibly solvent viscosity, could be evidence. Representative examples are superconductivity revealing a second-order phase transition as a function of temperature [95], integer-or-fractional quantum Hall effects as a function of external magnetic field and the current-voltage characteristics of hetero-junctions with double-wells/triple-barriers in AlGaAs/GaAs/AlGaAs/GaAs/AlGaAs devices [96].

Previously, we reported that several non-rigid chain-like Si-Si bond polymers (so-called helical polysilanes) which maintain rotational freedom of the Si-Si backbone in isooctane reveal discontinuous step-like helix-helix transition characteristics as a function of thermal energy bias. These helical polysilanes exhibited preferential (–)-sign CD signals in the magnitudes at most ~10 % below the helix-helix coalescence temperature ( $T_c$ ) regardless of the (S)- or (R)-chirality of the 3,7-dimethyloctyl side chains [58,59]. Similarly, in all cases of non-rigid luminophoric enantiomers, step-like and/or discontinuous transition behavior of (–)-CPL signals as a function of solvent viscosity could be evidence of unidirectional resonance tunneling induced by the PV-WNC. The greatest  $g_{lum}$  value ( $-1.5 \times 10^{-3}$ ) (Figure 13b) corresponds to 0.075 % excess of right-handed circular polarization of light over left-handed (as seen from the observer).

The origin of the negative sign could be due to the postulated WNC with the universal handedness and is similar to the observed sign in APV experiments. According to PV-WNC force ideas, parity-odd rotational motion enforces both (R)- and (S)-forms in the same direction clockwise (or counterclockwise) facilitating radiation of (–)-sign CPL. On the other hand, the parity-conserved parity-even EM force allows multiple C-C bonds in the (R)-form to rotate with clockwise motion, and conversely, those with the (S)-form to rotate counterclockwise or *vice versa*. These motional dynamics are mirror symmetric. From our experiences, we can group the apparent CPL and CD spectral characteristics with their signs, magnitudes and wavelengths into four categories:

(i) Case 1. The value of  $E_b$  between rigid enantiomers is sufficiently high, for example,  $> 30 \text{ kcal mol}^{-1}$  in the  $S_0$  and  $S_1$  state. In these cases, mirror-image CD and CPL spectra are apparent for the enantiomers. The parity-conserved (left-right equality or parity-even operational EM term) force is a deterministic factor. Such examples are D-10/L-10 and (R)-11/(S)-11 (Figure 3a–d).

(ii) Case 2. When  $10 < E_b < 30 \text{ kcal mol}^{-1}$  at the  $S_0$  and  $S_1$  states, one can observe non-mirror-image CPL and CD spectra. Although (+)- and (–)-signs in CPL and CD are primarily determined by molecular point and atropo chirality, the absolute magnitudes and wavelengths at vibronic CPL and CD bands are significantly different from each other. Such CPL spectra can be seen in (R)-12/(S)-12 dissolved in alkanols (Figure 3i–l) and (R)-13/(S)-13 in *n*-pentane (Figure 3m). Several papers have been published describing such non-mirror-image CPL and CD spectra [58–60,71,87].

(iii) Case 3. When  $1 < E_b < 10 \text{ kcal mol}^{-1}$  at the  $S_1$  and  $S_0$  states, only (–)-sign CPL and (–)-sign CD spectra were observed. The parity non-conserved weak force is a determining factor at the  $S_1$  and  $S_0$  states. No such examples revealing only (–)-sign CPL associated with (–)-sign CD spectra have been reported yet.

(iv) Case 4. When  $0 < E_b < 1 \text{ kcal mol}^{-1}$  at the  $S_1$  and  $S_0$  states, no CD bands were observed, although (–)-sign CPL was apparent. Parity-non-conserved (left-right inequality or parity-odd operational weak force) is deterministic factor in the  $S_1$  state, while the parity-conserved force (parity-even EM term permitting left-right equality) is deterministic in the  $S_0$  state. The value of  $1 \text{ kcal mol}^{-1}$  is arbitrary but representative for the rotational barrier of single bonds. Many examples of such cases are described in this paper.

Indeed, our experimental demonstration here might be a possible answer to the greatest mystery of the L-R preference on Earth based on the MPV hypothesis inferred by PV-WNC scenario. The key is to utilize a series of well-defined fluorophores available commercially in achiral solvents. This idea enables anyone to reproduce our results using a well-maintained commercial or home-made CPL spectrometer and associated CD spectrometer at any place at any time. We eagerly await further theoretical studies treating the time-evolutional behavior of photoexcited molecular systems.

Other cogent arguments for the L-R preference in the framework of the parity-conserved EM force and cosmological scale origins are possible. The photoexcited handedness of non-rigid molecules in a small % *ee* should increase to ~100% *ee* in the ground state according to several nonlinear amplification scenarios [97–107], for example, autocatalytic self-replication [97,98], sergeant-and-soldier and majority rule polymer cases [99], polymerization [100] and helix-helix transitions [101]. In addition to the fundamental question of charge-parity-time criteria (the so-called, conservation of CPT theorem) [102],

anti-neutrinos (left-handed as seen from the observer) of cosmological origin interacting with  $^{14}\text{N}$  in molecular clouds in star-forming regions of supernovae and neutron stars [103,104], parity violation of gravitational origin [105,106] and thermodynamic swirling flows in the north and south hemispheres on Earth [107] are of particular interest and might deserve to be used to verify these hypotheses in the future.

#### 4. Materials and Methods

Instrumentation details, lists of luminophores and solvents associated with vendors [63–65], preparation of sample solutions and chiroptical analytical data [71,108] are as below:

##### 4.1. Instrumentation

The CD and UV-visible spectra of the solution were recorded simultaneously at room temperature using a JASCO (Tokyo, Japan) J-820 spectropolarimeter using a cylindrical quartz cuvette with path lengths of 10 mm at ambient temperature. The cylindrical cuvette guaranteed a precision CD measurement compared to rectangular cuvettes that were often used in routine experiments. To obtain the precision CD/UV-visible spectra, a scanning rate of 50 and 100  $\text{nm min}^{-1}$ , a bandwidth of 2 nm, a response time of 2 s and 1 or 2 accumulations were employed. The instrument was fully aging at least 2 h to minimize unknown drifts of power supply and light source. Similarly, CPL and PL spectra were collected on a JASCO CPL-200 spectrofluoropolarimeter (Hachioji, Tokyo, Japan) using the cylindrical quartz cuvette with path lengths of 10 mm at room temperature. The optimal experimental parameters were that scanning rate: 20–50  $\text{nm min}^{-1}$ ; bandwidth: 10 nm for excitation and detection; response time of PMT: 8–16 s during measurements and 2-to-8 accumulations.

##### 4.2. Lists of Materials

###### 4.2.1. Luminophores (vendor)

Section 1: naphthalene (Sigma-Aldrich, St. Louis, MO, USA), anthracene (FUJIFILM Wako Pure Chemical Corporation, Osaka, Japan), tetracene (Tokyo Chemical Company (TCI), Tokyo, Japan), pyrene (Wako).

Section 2: 9,10-diphenylanthracene (Sigma-Aldrich), 9,10-bis(phenylethynyl)anthracene (TCI), 2,7-di-*tert*-butylpyrene (TCI), 1,3,6,8-tetraphenylpyrene (TCI), 5,12-bis(phenylethynyl)tetracene (Sigma-Aldrich).

Section 3: *D*-/*L*-camphor (Sigma-Aldrich), (*R*)-/*(S)*-(-)-1,1'-binaphthyl-2,2'-diyl hydrogen phosphate (TCI), (*R*)-/*(S)*-2,2'-dimethoxy-1,1'-binaphthyl (TCI), (*R*)-/*(S)*-2,2'-bis(methoxymethoxy)-1,1'-binaphthyl (TCI).

Section 4: biphenyl (TCI), *p*-terphenyl (TCI), *p*-quaterphenyl (TCI), *p*-quinquphenyl (TCI), *p*-hexaphenyl (TCI), DMT (Exciton, Tokyo Instruments Inc (Tokyo, Japan), Japanese vendor), TMQ (Exciton), QUI (Exciton), Exalite 360 (Exciton), TBS (Exciton), [12] cycloparaphenylene (Kanto Chemicals, Tokyo, Japan).

Section 5: 9,9-dimethylfluorene (TCI), 9,9-dioctylfluorene (TCI), Exalite384 (Exciton), 9,9-dihexylfluorene trimer (American Dye Source (ADS), Quebec, Canada), 9,9-dihexylfluorene pentamer (ADS), 9,9-dihexylfluorene heptamer (ADS), Exalite 376 (Exciton), Exalite 404 (Exciton), Exalite 428 (Exciton), Exalite 416 (Exciton).

###### 4.2.2. Solvents [Vendor, Viscosity in *cP* (Temperature in °C)]

(1) *n*-alkanes (in order of viscosity): *n*-pentane (FUJIFILM Wako, 0.21 (25)), *n*-hexane (FUJIFILM Wako, 0.30 (25)), *n*-heptane (Sigma-Aldrich, 0.39 (25)), *n*-octane (Sigma-Aldrich, 0.51 (25)), *n*-nonane (Sigma-Aldrich, 0.71 (20)), *n*-decane (Sigma-Aldrich, 0.85 (25)), *n*-undecane (Sigma-Aldrich, 0.93 (20)), *n*-dodecane (Sigma-Aldrich, 1.36 (25)), *n*-tridecane (Sigma-Aldrich, 1.88 (20)), *n*-tetradecane (Fluka, 2.08 (25)), *n*-pentadecane (Sigma-Aldrich, 2.86 (20)), *n*-hexadecane (Sigma-Aldrich, 3.71 (20))

(2) branched and cyclic alkanes (in order of viscosity): isooctane (Dotite, 0.50 (25)), cyclohexane (Dotite, 0.93 (22)), squalane (2,6,10,15,19,23-hexamethyltetracosane) (Sigma-Aldrich, 29.50 (25))

(3) Non-branched and *n*-alkanols (in order of viscosity): methanol (FUJIFILM Wako, 0.55 (25)), ethanol (FUJIFILM Wako, 1.09 (25)), *n*-propanol (Sigma-Aldrich, 1.96 (25)), *n*-butanol (FUJIFILM Wako, 2.59 (25)), *n*-pentanol (Sigma-Aldrich, 3.47 (25)), *n*-hexanol (Sigma-Aldrich, 4.59 (25)), *n*-heptanol (Wako, 5.97 (25)), *n*-octanol (Wako, 7.59 (25)), *n*-nonanol (Sigma-Aldrich, 9.51 (25)), *n*-decanol (Sigma-Aldrich, 11.50 (25)), ethylene glycol (FUJIFILM Wako, 16.1 (25)), *n*-undecanol (Sigma-Aldrich, 16.95 (25)), 1,3-propanediol (FUJIFILM Wako, 33.0 (25)), 1,4-butanediol (FUJIFILM Wako, 71.0 (25))

(4) branched alkanols (in order of viscosity): isopropanol (Dotite, 2.07 (25)), isobutanol (Sigma-Aldrich, 3.38 (25)), isopentanol (Sigma-Aldrich, 3.86 (25))

(5) chlorinated hydrocarbons (in order of viscosity): dichloromethane (Dotite, 0.41 (25)), chloroform (Dotite, 0.55 (25))

(6) Other solvents (in order of viscosity): diethyl ether (FUJIFILM Wako, 0.22 (25)), acetone (FUJIFILM Wako, 0.31 (25)), acetonitrile (FUJIFILM Wako, 0.34 (25)), tetrahydrofuran (Dotite, 0.46 (25)), benzene (FUJIFILM Wako, 0.60 (25)), *p*-dioxane (Dotite, 1.10 (25)), anisole (TCI, 1.09 (25)), sulfolane (TCI, 10.10 (25)).

#### 4.3. Preparation of Sample Solutions

First, a representatively stock solution ( $10^{-3}$  M) dissolved in spectroscopic grade  $\text{CHCl}_3$  (Dotite, Kumamoto, Japan) of luminophore was prepared. A small portion of the stock solution was injected to 1.9–2.1 mL of the desired liquid placed in the cylindrical quartz cuvette using a microsyringe, followed by manually shaking the mixture. Then, CPL/PL and CD/UV-vis spectra were measured.

#### 4.4. Chiroptical Analysis

The dissymmetry factor of circular polarization at the  $S_0$  state ( $g_{\text{abs}}$ ) was theoretically calculated as  $g_{\text{abs}} = (\varepsilon_L - \varepsilon_R) / [1/2(\varepsilon_L + \varepsilon_R)]$ , where  $\varepsilon_L$  and  $\varepsilon_R$  are the extinction coefficients for left- and right-CP light, respectively. The dissymmetry factor of circular polarization at the  $S_1$  state ( $g_{\text{lum}}$ ) was calculated as  $g_{\text{lum}} = (I_L - I_R) / [1/2(I_L + I_R)]$ , where  $I_L$  and  $I_R$  are the output signals for left- and right-circularly polarized light under the unpolarized incident light, respectively. The parameter  $g_{\text{abs}}$  was experimentally determined using the expression.

$\Delta\varepsilon/\varepsilon = [\text{ellipticity (in mdeg)} / 32,980] / \text{absorbance}$  at the CD extremum, similar to the parameter  $g_{\text{lum}}$ , which was calculated as  $\Delta I/I = [\text{ellipticity (in mdeg)} / (32,980 / \ln 10)] / [\text{total PL intensity (in Volts)}]$  at the CPL extremum.

### 5. Conclusions

We tested whether non-rigid,  $\pi$ -conjugated fluorophores in the  $S_1$  and  $S_0$  states in various achiral liquids with  $[\eta]$  ranging from 0.22 cP to 71.0 cP are optically inactive and mirror symmetrical by CPL and CD spectroscopy. The non-rigid luminophores included ten oligofluorene derivatives, eleven linear/cyclic oligo-*p*-phenylene derivatives, three binaphthyl derivatives, five fused aromatic rings (naphthalene, anthracene, tetracene, pyrene) with and without rotatable substituents. For comparison, we also tested unsubstituted naphthalene, anthracene, tetracene and pyrene as achiral planar fluorophores and a pair of camphor enantiomers as rigid chiral bicyclic fluorophores. We confirmed that the achiral rigid aromatic luminophores guaranteed no detectable CPL or CD signals and that camphor showed exactly mirror-image CPL and CD signals.

On the other hand, without exception, all the non-rigid fluorophoric enantiomers showed (–)-sign CPL signals emission from the vibronic photoexcited state, in support of the molecular parity-violating hypothesis according to the  $Z^0$ -boson origin PV-weak neutral current mechanism. Emission from these fluorophores increased progressively, discontinuously to  $\approx -(0.2 \text{ to } 2.0) \times 10^{-3}$  as a function of solvent viscosity. We believe that this behavior is as a consequence of satisfying the  $E_{\text{pv}} \sim E_{\pm}$  condition associated with resonance quantum tunneling. In a series of oligofluorenes, the  $g_{\text{lum}}$  value extrapolated

to zero-viscosity afforded a non-zero  $g_{lum}$  value, implying that the photoexcited oligofluorenes should emit (–)-sign CPL signals under collision-free vacuum conditions.

We found that an unpolarized low-energy (3–5 eV) light source generated handed chiral molecular species as observed by the emission of (–)-sign circularly polarized light in the UV-visible region when non-rigid racemic molecules with low barrier heights tested in this work were dissolved in achiral liquids, and even under collision-free vacuum conditions. Circularly and linearly polarized light sources may be not crucial.

**Supplementary Materials:** The following are available online, Figure S1: CPL/PL and CD/UV-vis spectral characteristics of pseudo- $D_{2h}$ -symmetrical fused aromatics carrying multiple rotatable substituents (6–9), Figure S2: CD/UV-vis and CPL/PL spectra of rigid binaphthol derivatives (*R*-11 and *S*-11) and semirigid binaphthol derivatives (*R*-12 and *S*-12), Figure S3: CPL/PL and CD/UV-Vis spectra of unsubstituted linear and cyclic oligo-*p*-phenyls (Ph3, Ph4, Ph5 and 12-CPP), Figure S4: CD/UV-vis and CPL/PL spectra of substituted linear oligo-*p*-phenyls (DMT, Exalite360, TMQ, QUI and TBS), Figure S5: CPL/PL and CD/UV-vis spectra of FL1-C<sub>1</sub> and FL1-C<sub>8</sub>, Figure S6: CPL/PL and CD/UV-vis spectra of FL2-C<sub>3</sub> (Exalite 384), Figure S7: CPL/PL and CD/UV-vis spectra of FL3-C<sub>6</sub> (fluorene trimer), Figure S8: CPL/PL and CD/UV-vis spectra of FL5-C<sub>6</sub> (fluorene pentamer), Figure S9: CPL/PL and CD/UV-vis spectra of FL7-C<sub>6</sub> (fluorene heptamer), Figure S10: Raw CPL/PL spectra of 2, *R*-11 and *S*-11 in chloroform and Exalite 428 in *n*-undecanol conducted by JASCO company at Tokyo with a CPL-300 spectrometer (16 November 2018 and 24 November 2018), Figure S11: Materials and methods including instrumentation, lists of materials, preparation of sample solutions and chiroptical analysis.

**Author Contributions:** M.F. with J.R.K. have considered many ideas in searching for verification of the *MPV* hypothesis over 20 years. M.F. designed the application of CPL/CD spectroscopy to test the *MPV* hypothesis of the  $\pi$ -conjugated luminophores. M.F., J.R.K., T.M. and Y.K. cowrote the manuscript. Requests for all original and processed CPL/CD data sets that are saved as several file formats [JASCO ##.jws, their converted ##.txt, followed by processed data using KaleidaGraph (mac, ver 4.53) ##.qpc and ##.qda] should be sent to M.F. (fujikim@ms.naist.jp).

**Funding:** This work was supported by Grants-in-Aid for Scientific Research [16H04155 (FY2016-2018), 23651092 (FY2014-2016), 22350052 (FY2010-2013), 16655046 (FY2003-2005)], the Sekisui Chemical Foundation [FY2009] and the NAIST Foundation [FY2009].

**Acknowledgments:** First of all, we owe a debt of gratitude to Reiko Kuroda (Tokyo Science of University) for giving us the opportunity to disclose our unpublished CPL/CD spectroscopic data sets accumulated at NAIST over 15 years to investigate the *MPV* hypothesis claimed by many theoreticians and experimentalists. Great inspiration for this work came from her intuitive book written in Japanese, titled ‘Seimei-Sekai-No-Hi-Taishosei’ [Broken Symmetry in the Biological World—Why Nature Loves Imbalance] (Chuko-Shinsho, Tokyo, Japan, 1992). We are grateful to the late Meir Shinitzky (Weizmann Institute of Science), Yosef Scolnik (Weizmann Institute of Science), Mikiharu Kamachi (Osaka University), Junji Watanabe (Tokyo Institute of Technology), Victor Borovkov (South-Central University for Nationalities, China), Katsuya Inoue (Hiroshima University), Ullrich Scherf (Bergische Universität Wuppertal), Masakatsu Matsumoto (Kanagawa University), Daisuke Uemura (Kanagawa University), Kazuo Yamaguchi (Kanagawa University), Nobuhiro Kihara (Kanagawa University), Takayoshi Kawasaki (Tokyo Institute of Technology, now, Tokuyama Corporation, Tsukuba), Anubhav Saxena (Momentive Inc. India, now Pidilite Industries, India), Tohru Asahi (Waseda University), Yoshio Okamoto (Nagoya University), Eiji Yashima (Nagoya University), Kenso Soai (Tokyo Science of University), Kenji Monde (Hokkaido University), Tamaki Nakano (Hokkaido University), Yoshitane Imai (Kindai University), Kento Okoshi (Chitose Institute of Science and Technology) and graduate students at NAIST, Fumiko Ichiyanagi, Masaaki Ishikawa, Yoshifumi Kawagoe, Yoko Nakano, Woojung Chung, Ayako Nakao, Kana Yoshida, Makoto Taguchi, Yuri Donguri, Nozomu Suzuki, Keisuku Yoshida, Yuka Kato, Shosei Yoshimoto, Duong Thi Sang, Yota Katsurada, Hiroki Kamite, Ai Yokokura, Nor Azura Abdul Rahim, Jalilah Binti Abd Jalil, Shun Okazaki and Nanami Ogata for critical comments and constructive discussion on the *MPV* hypothesis and our radical idea. Most of all students, several researchers (e.g., Puhup Puneet and Mohamed Mehawed Abdellatif) and Seiko Amazumi (technical staff) recognized inherent imbalance in chiroptical sign, magnitude and wavelength of non-rigid luminophores at our CPL-200 spectrometer even after a careful maintenance operated by a JASCO engineer, including replacement and tuning high-pressure Xenon light source, power supply, concave/flat mirror sets and two focused lenses. We are thankful to Takashi Takakuwa (JASCO), Yoshirou Kondo (JASCO), Hiroshi Kiyonaga (JASCO), Koushi Nagamori (JASCO) and Kenichi Akao (JASCO) for their intuitive and fruitful technical advice for many years and particular thanks are due to Nobuyuki Sakayanagi (JASCO), who designed the original CPL-200 spectrometer and released the first commercial model at the lab of M.F. in March 1999. Also thanks to Yasuo Nakanishi (JASCO Engineering), who continuously maintained the instrument in top condition with a high S/N ratio. Without such care and maintenance of the spectrometers, we could not test the *MPV* hypothesis. JASCO company independently verified partly our CPL/PL data (2 in chloroform, *R*-11/*S*-11 in chloroform and Exalite 428 in *n*-undecanol) by CPL-300 spectrometer (see, Figure S10 in SM). Finally, we thank three anonymous reviewers for careful reading our manuscript and many insightful comments.

**Conflicts of Interest:** The author has no competing interests or other interests that might be perceived to influence the results and/or discussion reported in this article.

## References

1. Janoschek, R. Theories on the origin of biomolecular Homochirality. In *Chirality—From Weak Bosons to the  $\alpha$ -Helix*; Janoschek, R., Ed.; Springer: Berlin, Germany, 1991; ISBN 978-3-642-76569-8.
2. Quack, M. Structure and dynamics of chiral molecules. *Angew. Chem. Int. Ed.* **1989**, *28*, 571–586. [[CrossRef](#)]
3. Hund, F. Symmetriecharaktere von Termen bei Systemen mit gleichen partikeln in der quantenmechanik. *Z. Phys.* **1927**, *43*, 788–803. [[CrossRef](#)]
4. Bunker, P.R.; Jensen, P. The symmetry groups of non-rigid molecules. In *Fundamentals of Molecular Symmetry*; Institute of Physics Publishing: Philadelphia, PA, USA, 2005; pp. 274–290. ISBN 0750309415.
5. Lee, T.D.; Yang, C.N. Question of parity conservation in weak interactions. *Phys. Rev.* **1956**, *104*, 254–258. [[CrossRef](#)]
6. Wu, C.S.; Ambler, E.; Hayward, R.W.; Hoppes, D.D.; Hudson, R.P. Experimental test of parity conservation on beta decay. *Phys. Rev.* **1957**, *105*, 1413–1415. [[CrossRef](#)]
7. Schopper, H. Circular polarization of  $\gamma$ -Rays: Further proof for parity failure in  $\beta$  Decay. *Philos. Mag.* **1957**, *2*, 710–713. [[CrossRef](#)]
8. Goldhaber, M.; Grodzins, L.; Sunyar, A. Helicity of neutrinos. *Phys. Rev.* **1958**, *109*, 1015–1017. [[CrossRef](#)]
9. Fagg, L.W.; Hanna, S.S. Polarization measurements on nuclear gamma rays. *Rev. Mod. Phys.* **1959**, *31*, 711–758. [[CrossRef](#)]
10. Wu, C.S. Parity experiments in beta decay. *Rev. Mod. Phys.* **1959**, *31*, 783–790. [[CrossRef](#)]
11. Electroweak Interaction. Available online: [https://en.wikipedia/wiki/Electroweak\\_interaction](https://en.wikipedia/wiki/Electroweak_interaction) (accessed on 28 July 2018).
12. Walgate, R. What will come after the  $Z^0$ ? *Nature* **1983**, *303*, 473. [[CrossRef](#)]
13. van der Meer, S. Stochastic cooling and the Accumulation of Antiprotons. *Rev. Mod. Phys.* **1985**, *57*, 689–698. [[CrossRef](#)]
14. Rubbia, C. Experimental observation of the intermediate vector bosons  $W^+$ ,  $W^-$  and  $Z^0$ . *Rev. Mod. Phys.* **1985**, *57*, 699–722. [[CrossRef](#)]
15. ENSDF Decay Data in the MIRD (Medical Internal Radiation Dose) Format for  $^{60}\text{Co}$ . Available online: <https://www.orau:ptp/ptp%20library/library/doe/bnl/nuclidedata/mirco60.htm> (accessed on 8 October 2018).
16. ENSDF Decay Data in the MIRD (Medical Internal Radiation Dose) Format for  $^{58}\text{Co}$ . Available online: <https://www.orau:ptp/ptp%20library/library/doe/bnl/nuclidedata/mirco58.htm> (accessed on 8 October 2018).
17. Bouchiat, M.A.; Bouchiat, C.C. Weak neutral currents in atomic physics. *Phys. Lett. B* **1974**, *48*, 111–114. [[CrossRef](#)]
18. Close, E.E. Parity violation in atoms? *Nature* **1976**, *264*, 505–506. [[CrossRef](#)]
19. Baied, P.E.G.; Brimcombe, M.W.S.; Roberts, G.J.; Sandars, P.G.H.; Soreide, D.C.; Fortson, E.N.; Lewis, L.L.; Lindahl, E.G.; Soreide, D.C. Search for parity non-conserving optical rotation in atomic bismuth. *Nature* **1976**, *264*, 528–529. [[CrossRef](#)]
20. Bucksbaum, P.H.; Commins, E.D.; Hunter, L.R. Observations of parity nonconservation in atomic thallium. *Phys. Rev. D* **1981**, *24*, 1134–1148. [[CrossRef](#)]
21. Emmons, T.P.; Reeves, J.M.; Fortson, E.N. Parity-nonconserving optical rotation in atomic lead. *Phys. Rev. Lett.* **1983**, *51*, 2089–2091. [[CrossRef](#)]
22. Bouchiat, M.-A.; Pottier, L. Optical experiments and weak interactions. *Science* **1986**, *234*, 1203–1210. [[CrossRef](#)] [[PubMed](#)]
23. *Parity Violation in Atoms and Polarized Electron Scattering*; Bernard, F.; Bouchiat, M.-A. (Eds.) World Scientific: Singapore, 1999; ISBN 9810237316.
24. Guéna, J.; Lintz, M.; Bouchiat, M.-A. Atomic parity violation: Principles, recent results, present motivations. *Mod. Phys. Lett. A* **2005**, *20*, 375–390. [[CrossRef](#)]
25. Okun, L.B. Mirror particles and mirror matter: 50 years of speculation and search. *Phys. Usp.* **2007**, *50*, 380–389. [[CrossRef](#)]
26. Tsigutkin, K.; Dounas-Frazer, D.; Family, A.; Stalnaker, J.E.; Yashchuk, V.V.; Budker, D. Observation of a large atomic parity violation effect in ytterbium. *Phys. Rev. Lett.* **2009**, *103*, 071601. [[CrossRef](#)] [[PubMed](#)]



27. Forte, M.; Heckel, B.R.; Ramsey, N.F.; Green, K.; Greene, G.L.; Byrne, J.; Pendlebury, J.M. First measurement of parity-nonconserving neutron-spin rotation: The tin isotopes. *Phys. Rev. Lett.* **1980**, *45*, 2088–2091. [[CrossRef](#)]
28. Yamagata, Y. A hypothesis for the asymmetric appearance of biomolecules on earth. *J. Theoret. Biol.* **1966**, *11*, 495–498. [[CrossRef](#)]
29. Rein, D.W. Some remarks on parity violating effects of intramolecular interactions. *J. Mol. Evol.* **1974**, *4*, 15–22. [[CrossRef](#)] [[PubMed](#)]
30. Letokhov, V.S. On difference of energy levels of left and right molecules due to weak interactions. *Phys. Lett. A* **1975**, *53*, 275–276. [[CrossRef](#)]
31. Keszthelyi, L. Chemical evolution: Effect of high energy radiation. *Orig. Life* **1976**, *7*, 349–354. [[CrossRef](#)] [[PubMed](#)]
32. Zel'Dovich, Y.B.; Saakyan, D.B.; Sobel'man, I.I. Energy difference between right-hand and left-hand molecules due to parity nonconservation in weak interactions of electrons with nuclei. *JETP Lett.* **1977**, *25*, 94–97.
33. Keszthelyi, L. Origin of the asymmetry of biomolecules and weak interaction. *Orig. Life* **1977**, *8*, 299–340. [[CrossRef](#)] [[PubMed](#)]
34. Harris, R.A.; Stodolsky, L. Quantum beats in optical activity and weak interactions. *Phys. Lett. B* **1978**, *78*, 313–317. [[CrossRef](#)]
35. Hegstrom, R.A.; Rein, D.W.; Sandars, P.G.H. Calculation of the parity nonconserving energy difference between mirror-image molecules. *J. Chem. Phys.* **1980**, *73*, 2329–2341. [[CrossRef](#)]
36. Mason, S.F.; Tranter, G.E. Energy inequivalence of peptide enantiomers from parity non-conservation. *Chem. Commun.* **1983**, 117–119. [[CrossRef](#)]
37. Hegstrom, R.A. Parity Nonconservation and the origin of biological chirality: Theoretical calculations. *Orig. Life* **1984**, *14*, 1–4. [[CrossRef](#)]
38. Mason, S.F. Origins of biomolecular handedness. *Nature* **1984**, *311*, 19–23. [[CrossRef](#)] [[PubMed](#)]
39. Mason, S.F.; Tranter, G.E. The electroweak origin of biomolecular handedness. *Proc. R. Soc. Lond. A* **1985**, *397*, 45–65. [[CrossRef](#)]
40. Hegstrom, R.A.; Kondepudi, D.K. The handedness of the universe. *Sci. Am.* **1990**, *262*, 108–115. [[CrossRef](#)]
41. Salam, A. The role of chirality in the origin of life. *J. Mol. Evol.* **1991**, *33*, 105–113. [[CrossRef](#)]
42. Macdermott, A.J. Electroweak enantioselection and the origin of life. *Orig. Life Evol. Biosph.* **1995**, *25*, 191–199. [[CrossRef](#)] [[PubMed](#)]
43. Kikuchi, O.; Kiyonaga, H. Parity-violating energy shift of helical *n*-alkanes. *J. Mol. Struct. (Theochem.)* **1994**, *312*, 271–274. [[CrossRef](#)]
44. Bonner, W.A. Enantioselective autocatalysis. IV. implications for parity violation effects. *Orig. Life Evol. Biosph.* **1996**, *26*, 27–45. [[CrossRef](#)] [[PubMed](#)]
45. Szabó-Nagy, A.; Keszthelyi, L. Demonstration of the parity-violating energy difference between enantiomers. *Proc. Natl. Acad. Sci. USA* **1999**, *96*, 4252–4255. [[CrossRef](#)] [[PubMed](#)]
46. Gottselig, M.; Luckhaus, D.; Quack, M.; Stohner, J.; Willeke, M. Mode selective stereomutation and parity violation in disulfane isotopomers H<sub>2</sub>S<sub>2</sub>, D<sub>2</sub>S<sub>2</sub>, T<sub>2</sub>S<sub>2</sub>. *Helv. Chim. Acta* **2001**, *84*, 1846–1861. [[CrossRef](#)]
47. Schwerdtfeger, P.; Gierlich, J.; Bollwein, T. Large parity-violation effects in heavy-metal-containing chiral compounds. *Angew. Chem. Int. Ed.* **2003**, *42*, 1293–1296. [[CrossRef](#)] [[PubMed](#)]
48. MacDermott, A.J.; Hegstrom, R.A. A proposed experiment to measure the parity-violating energy difference between enantiomers from the optical rotation of chiral ammonia-like “Cat” molecules. *Chem. Phys.* **2004**, *305*, 55–68. [[CrossRef](#)]
49. Quack, M.; Stohner, J.; Willeke, M. High-resolution spectroscopic studies and theory of parity violation in chiral molecules. *Annu. Rev. Phys. Chem.* **2008**, *59*, 741–769. [[CrossRef](#)] [[PubMed](#)]
50. Darquié, B.; Stoeffler, C.; Shelkovnikov, A.; Daussy, C.; Amy-Klein, A.; Chardonnet, C.; Zrig, S.; Guy, L.; Crassous, J.; Soulard, P.; et al. Progress toward the first observation of parity violation in chiral molecules by high-resolution laser spectroscopy. *Chirality* **2010**, *22*, 870–884. [[CrossRef](#)] [[PubMed](#)]
51. Dorta-Urra, A.; Peñate-Rodríguez, H.C.; Bargaño, P.; Rojas-Lorenzo, G.; Miret-Artés, S. Dissipative geometric phase and decoherence in parity-violating chiral molecules. *J. Chem. Phys.* **2012**, *136*, 174505, (6 pages). [[CrossRef](#)] [[PubMed](#)]

52. Albert, S.; Arn, F.; Bolotova, I.; Chen, Z.; Fábri, C.; Grassi, G.; Lerch, P.; Quack, M.; Seyfang, G.; Wokaun, A.; et al. Synchrotron-based highest resolution terahertz spectroscopy of the  $\nu_{24}$  band system of 1,2-dithiine ( $C_4H_4S_2$ ): A candidate for measuring the parity violating energy difference between enantiomers of chiral molecules. *J. Phys. Chem. Lett.* **2016**, *7*, 3847–3853. [CrossRef] [PubMed]
53. Daussy, C.; Marrel, T.; Amy-Klein, A.; Nguyen, C.T.; Bordé, C.J.; Chardonnet, C. Limit on the parity nonconserving energy difference between the enantiomers of a chiral molecule by laser spectroscopy. *Phys. Rev. Lett.* **1999**, *83*, 1554–1557. [CrossRef]
54. Viedma, C. Selective chiral symmetry breaking during crystallization: Parity violation or cryptochiral environment in control? *Cryst. Growth Des.* **2007**, *7*, 553–556. [CrossRef]
55. Wang, W.; Yi, F.; Ni, Y.; Zhao, Z.; Jin, X.; Tang, Y. Parity violation of electroweak force in phase transitions of single crystals of D- and L-alanine and valine. *J. Biol. Phys.* **2000**, *26*, 51–65. [CrossRef] [PubMed]
56. Scolnik, T.; Portnaya, I.; Cogan, U.; Tal, S.; Haimovitz, R.; Fridkin, M.; Elitzur, A.C.; Deamer, D.W.; Shinitzky, M. Subtle differences in structural transitions between poly-L- and poly-D-amino acids of equal length in water. *Phys. Chem. Chem. Phys.* **2006**, *8*, 333–339. [CrossRef] [PubMed]
57. Kodona, E.K.; Alexopoulos, C.; Panou-Pomonis, E.; Pomonis, P.J. Chirality and helix stability of polyglutamic acid enantiomers. *J. Colloid Interface Sci.* **2008**, *319*, 72–80. [CrossRef] [PubMed]
58. Fujiki, M. Experimental tests of parity violation at helical polysilylene level. *Macromol. Rapid Commun.* **2001**, *22*, 669–674. [CrossRef]
59. Fujiki, M. Mirror symmetry breaking in helical polysilanes: Preference between left and right of chemical and physical origin. *Symmetry* **2010**, *2*, 1625–1652. [CrossRef]
60. Fujiki, M.; Kawagoe, Y.; Nakano, Y.; Nakao, A. Mirror-symmetry-breaking in poly[(9,9-di-*n*-octylfluorenyl-2,7-diyl)-*alt*-biphenyl] (PF8P2) is susceptible to terpene chirality, achiral solvents and mechanical stirring. *Molecules* **2013**, *18*, 7035–7057. [CrossRef] [PubMed]
61. Gabuda, S.P.; Kozlova, S.G. Chirality-related interactions and a mirror symmetry violation in handed nano structures. *J. Chem. Phys.* **2014**, *141*, 044701. [CrossRef] [PubMed]
62. Kozlova, S.G.; Gabuda, S.P. Thermal properties of  $Zn_2(C_8H_4O_4)_2 \cdot C_6H_{12}N_2$  Metal-organic framework compound and mirror symmetry violation of dabco molecules. *Sci. Rep.* **2017**, *7*, 11505. [CrossRef] [PubMed]
63. Lide, D.R. *Handbook of Organic Solvents*; CRC Press: Boca Raton, FL, USA, 1994; ISBN 0849389305.
64. Viswanath, D.S.; Ghosh, T.; Prasad, D.H.L.; Dutt, N.V.K.; Rani, K.Y. *Viscosity of Liquids*; Theory, Estimation, Experiment and Data. Springer: Berlin, Germany, 2007; ISBN 9048173787.
65. Properties of Organic Solvents. Available online: <http://murov.info/orgsolvents.htm>. (accessed on 12 June 2018).
66. Turro, N.J. *Modern Molecular Photochemistry*; University Science Books: Sausalito, CA, USA, 1991; ISBN 0935702717.
67. Calvert, J.G.; Pitts, J.N. *Photochemistry*; John Wiley & Sons: Hoboken, NJ, USA, 1973; ISBN 0471130907.
68. Shindo, Y.; Nakagawa, M. On the artifacts in circularly polarized emission spectroscopy. *Appl. Spectrosc.* **1985**, *39*, 32–38. [CrossRef]
69. Blok, P.M.L.; Dekkers, H.P.J.M. Measurement of the circular polarization of the luminescence of photoselected samples under artifact-free conditions. *Appl. Spectrosc.* **1990**, *44*, 305–309. [CrossRef]
70. Longhi, G.; Castiglioni, E.; Abbate, S.; Lebon, F.; Lightner, D.A. Experimental and calculated CPL spectra and related spectroscopic data of camphor and other simple chiral bicyclic ketones. *Chirality* **2013**, *25*, 589–599. [CrossRef] [PubMed]
71. Thi Duong, S.; Fujiki, M. The origin of bisignate circularly polarized luminescence (CPL) spectra from chiral Polymer aggregates and molecular camphor: Anti-kasha's rule revealed by CPL excitation (CPLE) spectra. *Polym. Chem.* **2017**, *8*, 4673–4679. [CrossRef]
72. Kinuta, T.; Sato, T.; Nakano, Y.; Harada, T.; Tajima, N.; Fujiki, M.; Kuroda, R.; Matsubara, Y.; Imai, Y. Solid-state chiral optical properties of axially chiral binaphthyl acid derivatives. *J. Photochem. Photobiol. A Chem.* **2011**, *220*, 134–138. [CrossRef]
73. Kimoto, T.; Tajima, N.; Fujiki, M.; Imai, Y. Control of circularly polarized luminescence by using open and closed-type binaphthyl derivatives with the same axial chirality. *Chem.–Asian J.* **2012**, *7*, 2836–2841. [CrossRef] [PubMed]
74. Kinuta, T.; Tajima, N.; Fujiki, M.; Miyazawa, M.; Imai, Y. Control of circularly polarized photoluminescent property via dihedral angle of binaphthyl derivatives. *Tetrahedron* **2012**, *68*, 4791–4796. [CrossRef]

75. Amako, T.; Kimoto, T.; Tajima, N.; Fujiki, M.; Imai, Y. A comparison of circularly polarized luminescence (CPL) and circular dichroism (CD) characteristics of four axially chiral binaphthyl-2,2'-diyl hydrogen phosphate derivatives. *Tetrahedron* **2013**, *69*, 2753–2757. [CrossRef]
76. Schneider, D.J.; Landis, D.A.; Fleitz, P.A.; Seliskar, C.J.; Kauffman, J.M.; Steppel, R.N. Characterization of new excimer pumped UV laser dyes I. *p-terphenyls*, *Laser Chem.* **1991**, *11*, 49–62. [CrossRef]
77. Fleitz, P.A.; Seliskar, C.J.; Steppel, R.N.; Kauffman, J.M.; Kelley, C.J.; Ghiorghis, A. Characterization of new excimer pumped UV laser dyes 2. *p-quaterphenyls*, *Laser Chem.* **1991**, *11*, 99–107. [CrossRef]
78. Seliskar, C.J.; Landis, D.A.; Kauffman, J.M.; Aziz, M.A.; Steppel, R.N.; Kelley, C.J.; Qin, Y.; Ghiorghis, A. Characterization of new excimer pumped UV laser dyes 3. *p-quinqui-, sexi-, octi- and deciphenyls*. *Laser Chem.* **1993**, *13*, 19–28. [CrossRef]
79. Omachi, H.; Segawa, Y.; Itami, K. Synthesis of cycloparaphenylenes and related carbon nanorings: A step toward the controlled synthesis of carbon nanotubes. *Acc. Chem. Res.* **2012**, *45*, 1378–1389. [CrossRef] [PubMed]
80. Omachi, H.; Nakayama, T.; Takahashi, E.; Segawa, Y.; Itami, K. Initiation of carbon nanotube growth by well-defined carbon nanorings. *Nat. Chem.* **2013**, *5*, 572–576. [CrossRef] [PubMed]
81. Monkman, A.; Rothe, C.; King, S.; Dias, F. Polyfluorene photophysics. *Adv. Polym. Sci.* **2008**, *212*, 187–225. [CrossRef]
82. Klaerner, G.; Miller, R.D. Polyfluorene derivatives: Effective conjugation lengths from well-defined oligomers. *Macromolecules* **1998**, *31*, 2007–2009. [CrossRef]
83. Shiraki, T.; Shindome, S.; Toshimitsu, F.; Fujigaya, T.; Nakashima, N. Strong main-chain length-dependence for the  $\beta$ -phase formation of oligofluorenes. *Polym. Chem.* **2015**, *6*, 5103–5109. [CrossRef]
84. Kondepudi, D. Parity violations and the origin of bimolecular handedness. In *Entropy, Information and Evolution: New Perspective on Physical and Biological Evolution*; Weber, B.H., Depew, D.J., Smith, J.D., Eds.; MIT Press: Cambridge, MA, USA, 1988; ISBN 0262731681.
85. Shinitzky, M. Configurational entropy in chiral solutions—Negative entropy of solvent envelopes. *Entropy* **2009**, *11*, 667–674. [CrossRef]
86. Shinitzky, M. Space asymmetry as a possible global feature. *Chirality* **2013**, *25*, 308–311. [CrossRef] [PubMed]
87. Wang, L.; Suzuki, N.; Liu, J.; Matsuda, T.; Rahim, N.A.A.; Zhang, W.; Fujiki, M.; Zhang, Z.; Zhou, N.; Zhu, X. Limonene induced chiroptical generation and inversion during aggregation of achiral polyfluorene analogs: Structure-dependence and mechanism. *Polym. Chem.* **2014**, *5*, 5920–5927. [CrossRef]
88. Category: Proton-Proton Chain Reaction. Available online: [https://en.wikipedia/wiki/Proton--proton\\_chain\\_reaction](https://en.wikipedia/wiki/Proton--proton_chain_reaction) (accessed on 28 August 2018).
89. Arrow of Time. Available online: [https://en.wikipedia/wiki/Arrow\\_of\\_time](https://en.wikipedia/wiki/Arrow_of_time) (accessed on 15 September 2018).
90. Franck-Condon-Principle. Available online: [https://en.wikipedia/wiki/Franck--Condon\\_principle](https://en.wikipedia/wiki/Franck--Condon_principle) (accessed on 29 June 2018).
91. Guijarro, A.; Yus, M. *Origin of Chirality in the Molecules of life: A Revision from Awareness to the Current Theories and Perspectives of this Unsolved Problem*; RSC Publishing: Cambridge, UK, 2008; ISBN 978-0-85404-156-5.
92. Chronology of the Universe. Available online: [https://en.wikipedia/wiki/Chronology\\_of\\_the\\_universe](https://en.wikipedia/wiki/Chronology_of_the_universe) (accessed on 6 September 2018).
93. Freedman, R.; Geller, R.; Kaufmann, W.J. *Universe*, 10th ed.; Freeman, W.H., Ed.; W.H. Freeman and Company: London, UK, 2015; ISBN 1319042384.
94. Story of the Universe. Available online: <http://cms.web.cern.ch/content/story-universe> (accessed on 7 December 2011).
95. Superconductivity. Available online: <https://en.wikipedia/wiki/Superconductivity> (accessed on 24 August 2018).
96. Allford, C.P.; Legg, R.E.; O'Donnell, R.A.; Dawson, P.; Missous, M.; Buckle, P.D. Thermally activated resonant tunnelling in GaAs/AlGaAs triple barrier heterostructures. *Semicond. Sci. Technol.* **2015**, *30*, 105035. [CrossRef]
97. Avetisov, V.; Goldanskii, V. Mirror symmetry- breaking at the molecular level. *Proc. Natl. Acad. Sci. USA* **1996**, *93*, 11435–11442. [CrossRef] [PubMed]
98. Soai, K.; Kawasaki, T. Asymmetric autocatalysis with amplification of chirality. *Top. Curr. Chem.* **2008**, *284*, 1–33. [CrossRef]
99. Green, M.M.; Jain, V. Homochirality in life: Two equal runners, one tripped. *Orig. Life Evol. Biosph.* **2010**, *40*, 111–118. [CrossRef] [PubMed]

100. Sandars, P.G.H. A toy model for the generation of Homochirality during polymerization, *Orig. Life Evol. Biosph.* **2003**, *33*, 575–587. [[CrossRef](#)]
101. Fujiki, M. Mirror symmetry breaking of silicon polymers—From weak bosons to artificial helix. *Chem. Rec.* **2009**, *9*, 271–298. [[CrossRef](#)] [[PubMed](#)]
102. Barron, L.D. Symmetry and molecular chirality. *Chem. Soc. Rev.* **1986**, *15*, 189–223. [[CrossRef](#)]
103. Famiano, M.A.; Boyd, R.N.; Kajino, T.; Onaka, T.; Mo, Y. Amino acid chiral selection via weak interactions in stellar environments: Implications for the origin of life. *Sci. Rep.* **2018**, *8*, 8833. [[CrossRef](#)] [[PubMed](#)]
104. Bargeño, P.; de Tudela, R.P. The role of supernova neutrinos on molecular homochirality, *Orig. Life Evol. Biosph.* **2007**, *37*, 253–257. [[CrossRef](#)] [[PubMed](#)]
105. Alexander, S.; Marciànò, A.; Smolin, L. Gravitational origin of the weak interaction's chirality. *Phys. Rev. D* **2014**, *89*, 065017. [[CrossRef](#)]
106. Bargeño, P. Gravitational origin parity violation. *Chirality* **2015**, *27*, 375–381. [[CrossRef](#)] [[PubMed](#)]
107. Ribó, J.M.; Blanco, C.; Crusats, J.; El-Hachemi, Z.; Hochberg, D.; Moyano, A. Absolute asymmetric synthesis in enantioselective autocatalytic reaction networks: Theoretical games, speculations on chemical evolution and perhaps a synthetic option. *Chem. Eur. J.* **2014**, *20*, 17250–17271. [[CrossRef](#)] [[PubMed](#)]
108. Alez, G. *Circular Polarization: General Description, Circular Dichroism, Circularly Polarized Luminescence, Antennas, Circular Polarization of Nature*; Webster's Digital Services: Wahroonga, NSW, Australia, 2012; ISBN 127618848X.

**Sample Availability:** Samples of the compounds are not available from the authors.



© 2018 by the authors. Licensee MDPI, Basel, Switzerland. This article is an open access article distributed under the terms and conditions of the Creative Commons Attribution (CC BY) license (<http://creativecommons.org/licenses/by/4.0/>).